Journal of Statistical Software

MMMMMM YYYY, Volume VV, Issue II. doi: 10.18637/jss.v000.i00

A Flow-Driven Cavity as an Air Cycling Model for Window Flow

Justin Campbell **Amanda Hiett** **Akhil Sadam**

Abstract

A lid-driven cavity is flow-driven to describe stress on and circulation inside buildings and small insect-to-UAV-size aircraft due to open windows or sidewall punctures. The transition between steady & unsteady flow is also roughly bounded, by investigating the Reynolds number at 4 values between 10 to 10^4. A sparse simulation of low-speed and much higher-speed incompressible flows is undertaken, estimating feature shapes at the minimum computational cost.

Keywords: computational fluid dynamics, CFD, incompressible, Paraview, R, Python, coe347, spring 2022, window, building, tornado, high, reynolds, unsteady, steady, stress, strain, rate, mixing, volumetric, flow.

1. Motivation

For severe storms, it is widely known that puncture damage is the primary cause of failure for most buildings and aircraft. Once a puncture has been created, the resultant pressure differential can cause fast inflow and damage to the interior. We seek to study this inflow, and stresses near the opening walls, which can cause structural issues leading to collapse of one or more walls.

Most relevant studies use incredibly large amounts of computational power, due to the large scale of the problem (Reynolds numbers for tornadoes and hurricanes can easily start in the millions). We seek to show the applicability of lower Reynolds simulations to higher Reynolds situations, since the general large-scale flow structure remains the same.

2. Literature Review

Wind speeds may be categorized as dangerous once reaching the threshold of 50mph. Winds of this caliber may occur during storms and tornados, and can be catastrophic to infrastructure.(2019; Hadhazy 2011; Tessner 2021)

Structurally, windows are weak in comparison to the surrounding structure and therefore are generally the first to break when confronted with strong winds. The missing window then creates a cavity with a pressure differential to the outside wind that may encourage further destruction. The

fragility of windows is why many coastal buildings near hurricane hotspots have shutters, and in the event of a storm, those without shutters often cover their windows with materials such as plywood to protect against the oncoming winds.(2019; Hadhazy 2011; Tessner 2021)

The average home is designed to withstand winds of 90mph for around 3 seconds, which is far from sufficient to withstand even a moderate class of tornado. Especially when including forces working in tadem generating lift on top of normal stressors. As roof connections rely primarily on gravity to ensure stabiity, any opposing force to gravity need only overcome the weight force of the roof to remove it from the structure entirely.(2019; Hadhazy 2011; Tessner 2021)

Due to the propensity of air to create vortices when exposed to nonzero velocity and pressure differential, the way air may travel through the structure could pose an additional destructor on top of the exterior conditions. It has been proven advantageous for homes in storm-prone areas to install shutters, so prevention of inducing cavity-like flow on a structure is of import.(2019; Hadhazy 2011; Tessner 2021)

3. Implementation

We implement all simulation with OpenFoam, analysis with Paraview and Python3, and documentation code in R Xie, Dervieux, and Riederer (2020).

4. Mesh Assembly

We assemble a 2D mesh template as below, with the following parameters, all lengths nondimensionalized in terms of dimension L:

mutable: wall thickness w, window width a,
immutable: window location $b = 0.5$, cavity height $H = 1$, cavity width $L = 1$, and free-stream width $2e = 0.1$.

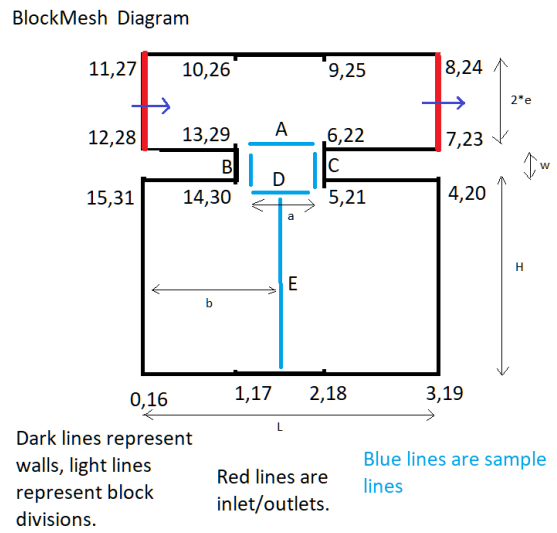

Two sets of simulations are performed, one for the low Reynolds (Re) numbers of 10 and 200, which will be shown to be steady, and another for $Re = 1000, 10000$.

Each mesh also has a corresponding refinement, which is described by the *meshFactor* parameter, representing the refinement in each dimension.

Full lists are available below.

4.1. Meshes for the Low Reynolds simulations

meshfactor	Reynolds	a	w
5	10	0.05	0.05
5	10	0.05	0.10
5	10	0.50	0.05
5	10	0.50	0.10
10	10	0.05	0.05
10	10	0.05	0.10
10	10	0.50	0.05
10	10	0.50	0.10
5	200	0.05	0.05
5	200	0.05	0.10
5	200	0.50	0.05
5	200	0.50	0.10
10	200	0.05	0.05
10	200	0.05	0.10
10	200	0.50	0.05
10	200	0.50	0.10

Table 1:

4.2. Meshes for the High Reynolds simulations

meshfactor	Reynolds	a	w
3	1000	0.5	0.1
5	1000	0.5	0.1
3	10000	0.5	0.1
5	10000	0.5	0.1

Table 2:

BlockMeshDict and similar files are available at the repository.

4.3. Mesh Images

A couple mesh samples are shown here; see the appendix for all images.

meshFactor, Re, windowWidth, wallThickness=5, 10, 0.05, 0.05:

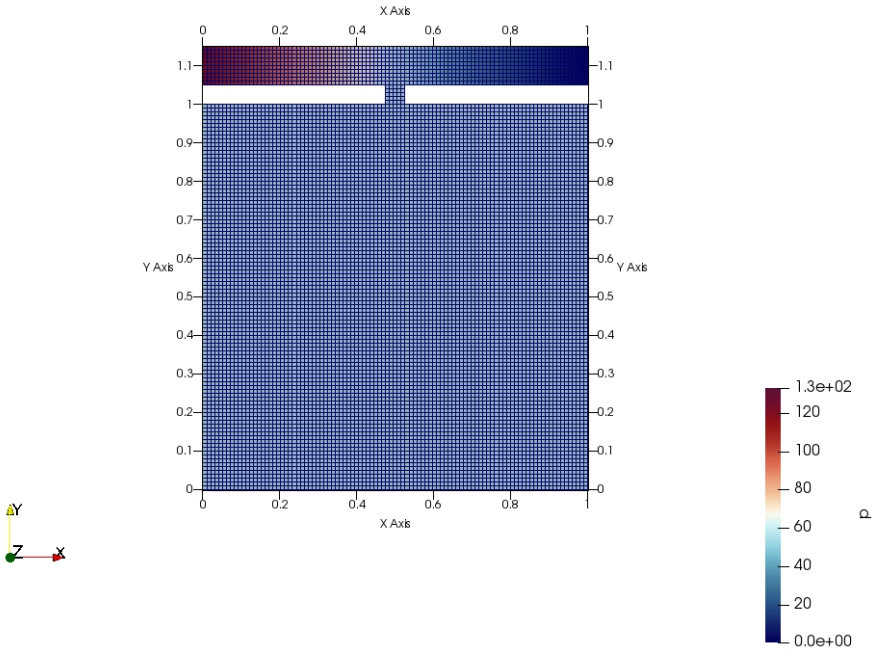

meshFactor, Re, windowWidth, wallThickness=10, 200, 0.5, 0.1:

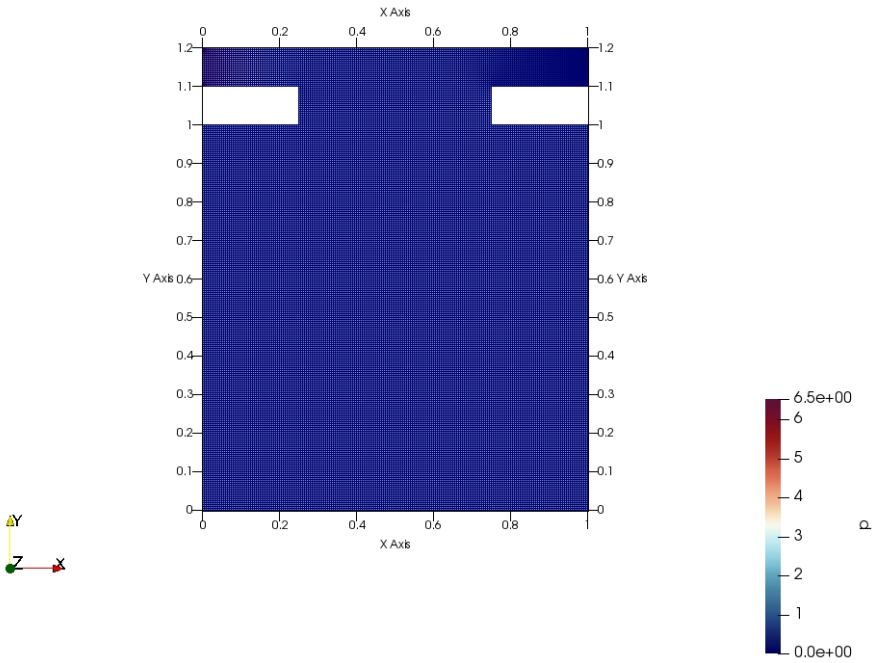

Now that the mesh resolutions can be seen as adequate, we will move to results.

5. Low Reynolds Number

Note all values are nondimensionalized - all lengths are in terms of L, the cavity length, all speeds in terms of U, the initial flow speed, and all times in terms of $\frac{L}{U}$.

The pressure is in terms of $\frac{p}{\rho U^2}$. All low-Reynolds simulations were run till T=6.

5.4. General Solution Form

We will now show the pressure, X-velocity, Y-velocity, and streamlines in sets of 4 by varying geometry along the following pattern. Contours are not shown due to their bias toward out-of-cavity portions and the coarse mesh will be omitted for brevity. Convergence studies will be done numerically afterward.

Pattern:

window.size.a	wall.thickness.w
0.05	0.05
0.05	0.10
0.50	0.05
0.50	0.10

Table 3:

Re=10, Pressure

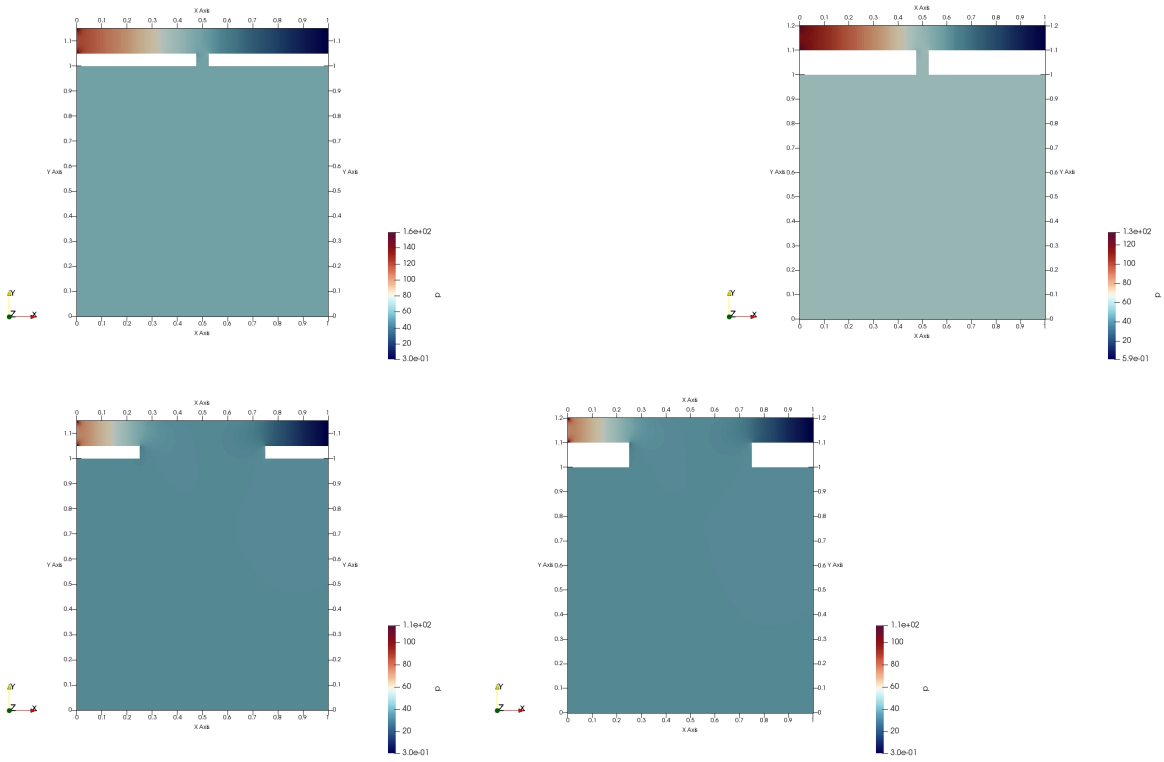

Note that all meshes have relatively even internal pressure, suggesting internal flow speeds are miniscule. Also, the more contact the cavity has with the crossflow, the lower the internal cavity pressure. Finally, consider the inlet. Note that the higher-pressure regions localize at the corners with larger windows, implying that the cavity acts as a sort of pressure sink.

Re=10, X-velocity

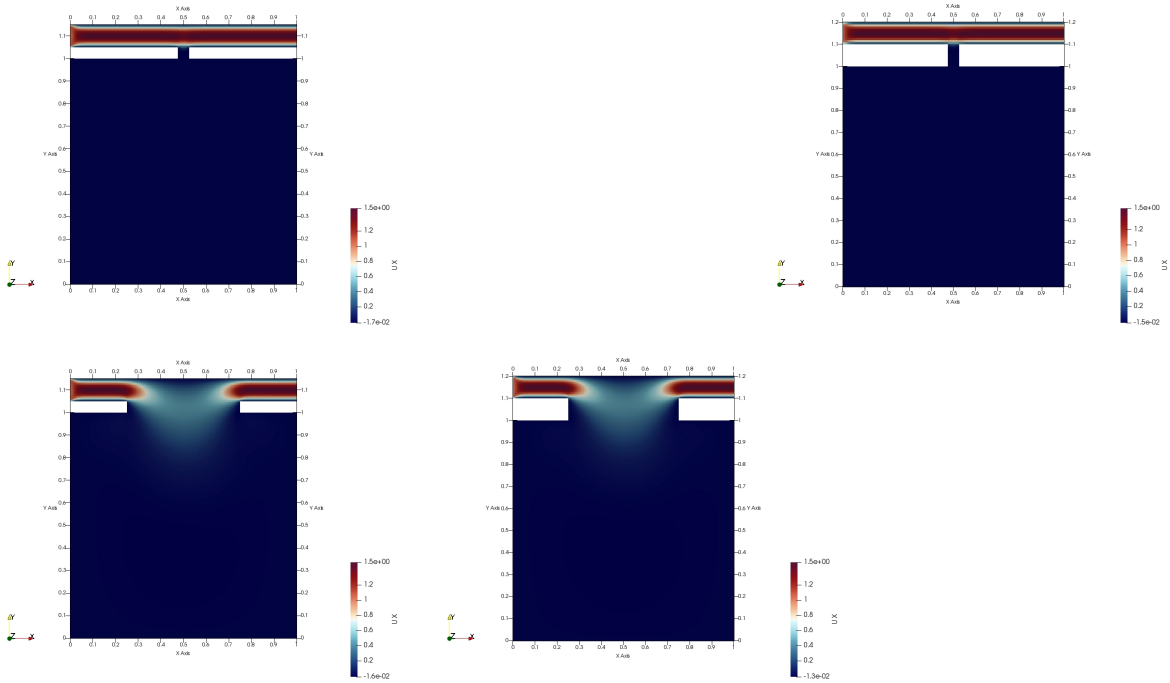

Similarly, the flow x-velocity dissipates across the window in amounts positively correlated with larger and thinner windows. No discernible cavity flow can be seen yet.

Re=10, Y-velocity

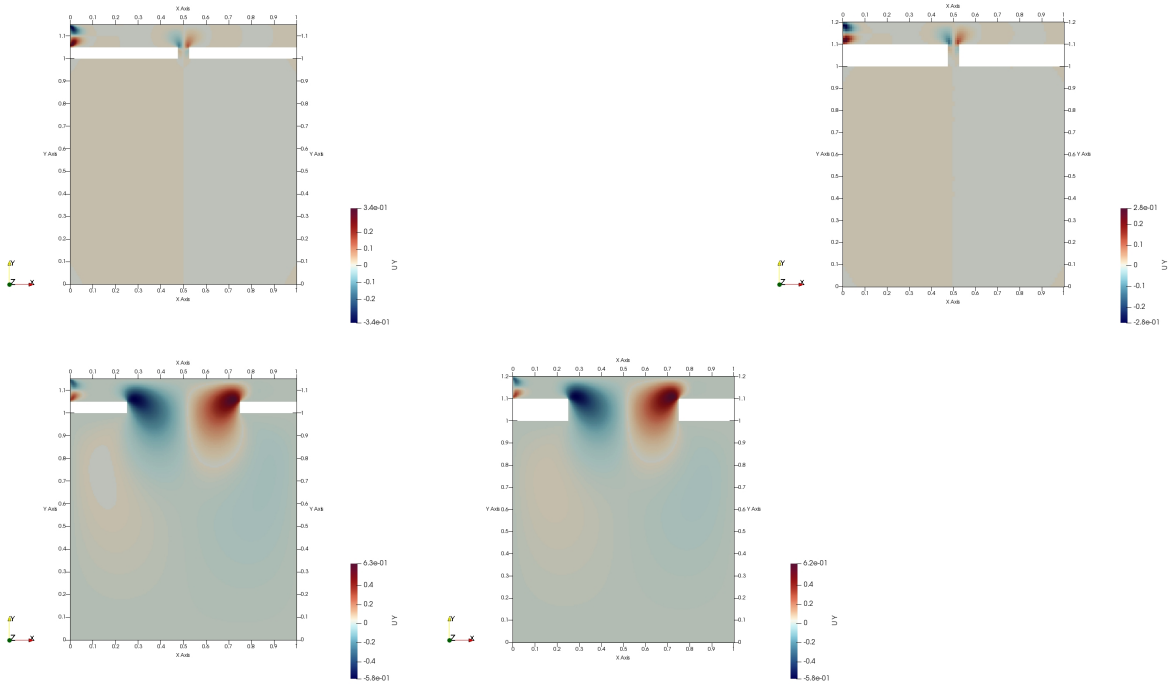

The same story can be seen in the y-velocities, but now there can be seen a cavity circulation (by the mild color differences inside the cavity). Note that the windows of 0.05 width produce really mild, near-complete cavity circulation, while the larger windows of 0.5 width produce much stronger but incomplete circulation (the corners are relatively unaffected).

Re=10, Streamlines

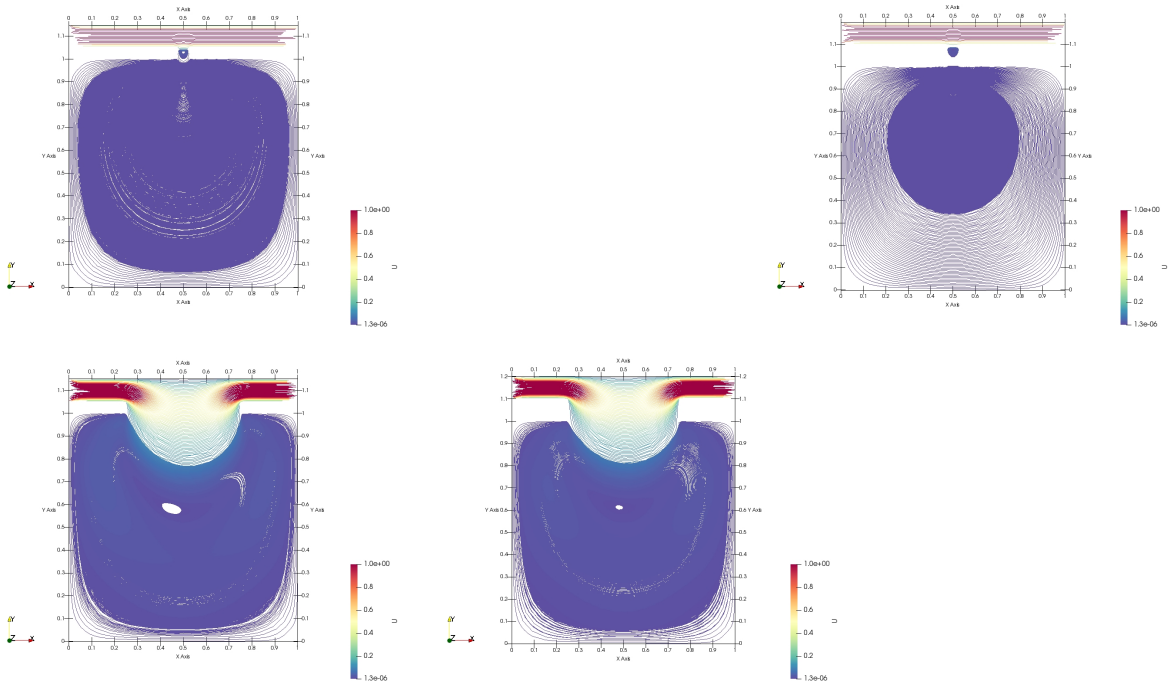

This is confirmed by the streamline plots. Note that there are between 1-3 transition vortices. At maximum, with the most neck-like window, there is a vortice the window opening, one in the window another in opening to the cavity. These three vortices connect the crossflow to the internal centralized vortex. When the window is broadened, these vortices all combine to form a single large transition vortice. Finally, note the center of the centralized vortice is very close to the center, and the crossflow bend is similarly symmetric, despite the flow directionality. This symmetry is probably due to the low Reynolds number of the flow.

Re=200, Pressure

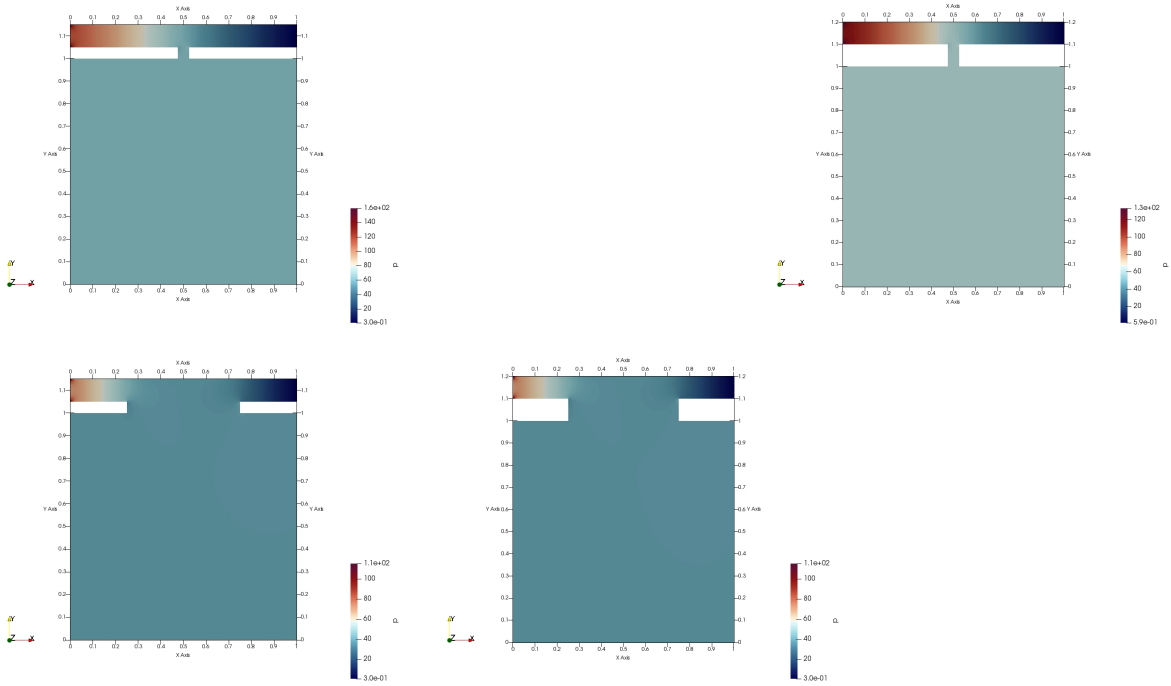

The pressure for Re=200 is very similar to that of Re=10 - the cavity acts like a simple pressure sink.

Re=200, X-velocity

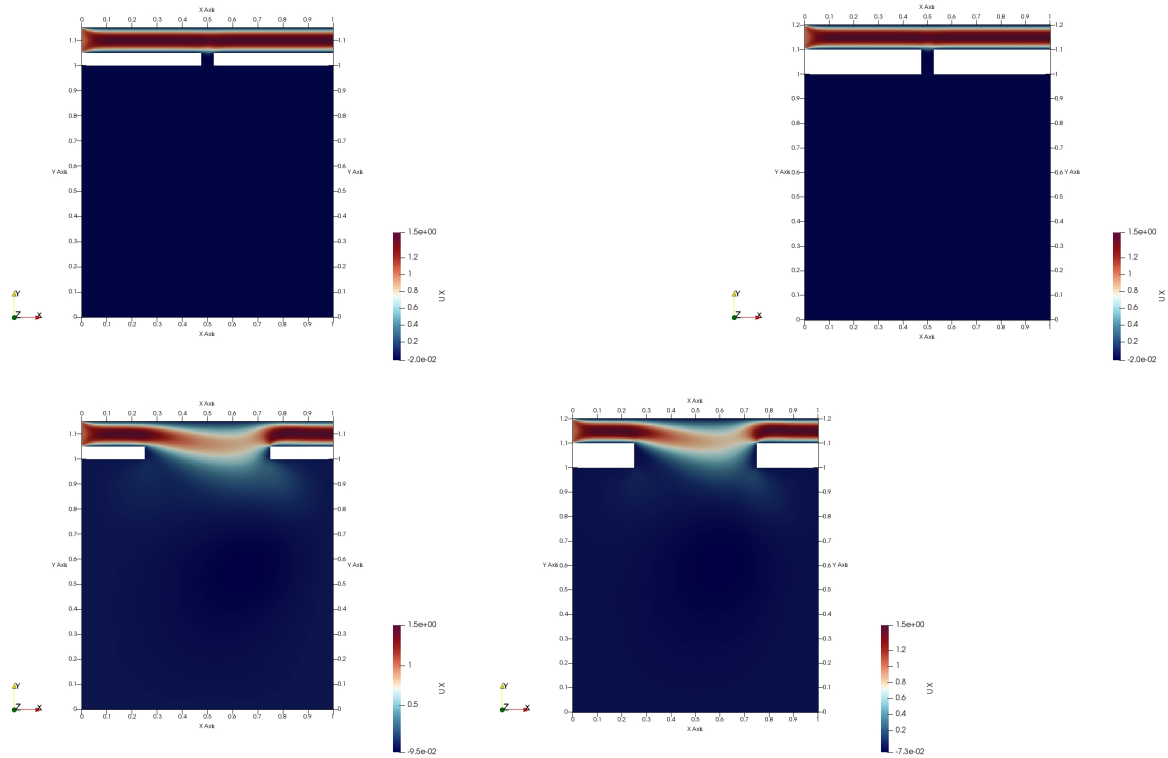

The only major difference is the asymmetry, which is probably due to the Reynolds number. Note that these solutions are also stable, and have been checked by flow visualization over time.

Re=200, Y-velocity

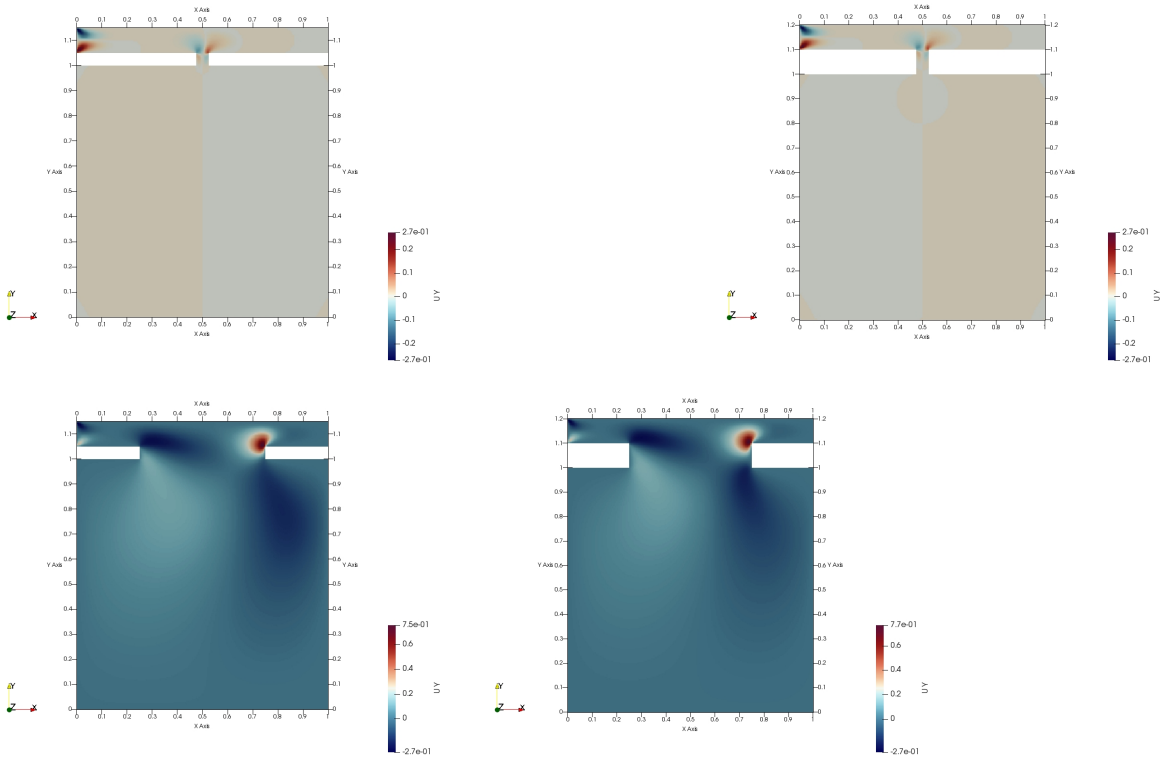

Note that in addition to the asymmetry (same as seen in the x-velocity plots), there is an additional hydraulic jump right at the upper-right window corner, as the flow resumes high speed.
We will return to this in the high Reynolds section, as with increasing Re, this sort of jump can cause additional effects. We can also see the prominent third transition vortice clearly in the top-right plot.

Re=200, Streamlines

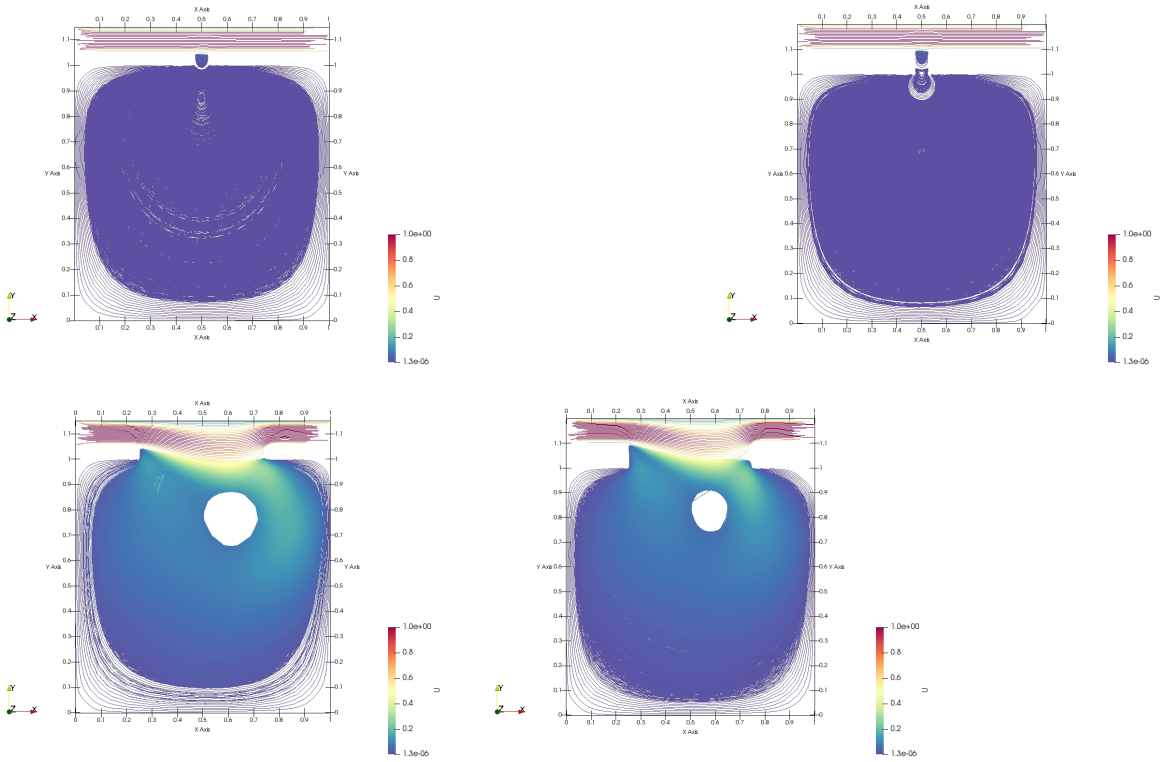

Note the prominent third transition vortice. Otherwise, everything is as expected from Re=10 flow, except for the asymmetry.

5.5. Vortice Positions

Convergence can easily be seen by looking at the centralized vortex position for both meshes, by differing geometry.

meshfactor	Reynolds	window.a.	wall.w.	Vortex.Center.Location.along.Y
5	10	0.05	0.05	0.8350
10	10	0.05	0.05	0.8525
5	10	0.05	0.10	0.9650
10	10	0.05	0.10	0.9650
5	10	0.50	0.05	0.5650
10	10	0.50	0.05	0.5725
5	10	0.50	0.10	0.6050
10	10	0.50	0.10	0.6075
5	50	0.05	0.05	0.8350
10	50	0.05	0.05	0.8525
5	50	0.05	0.10	0.9650
10	50	0.05	0.10	0.6075
5	50	0.50	0.05	0.6550
10	50	0.50	0.05	0.6625
5	50	0.50	0.10	0.6850
10	50	0.50	0.10	0.6875
5	200	0.05	0.05	0.8550
10	200	0.05	0.05	0.8675
5	200	0.05	0.10	0.9750
10	200	0.05	0.10	0.6875
5	200	0.50	0.05	0.7650
10	200	0.50	0.05	0.7725
5	200	0.50	0.10	0.8250
10	200	0.50	0.10	0.8325

Table 4:

5.6. Window Wall Solution Profiles

Now consider the profiles along the left and right window walls; the vertical segments along the inside of the window.

To examine the effect of changing the mesh geometry (wall thickness and window size), mesh resolution (mesh resize factor), and the unsteadiness of the flow (measured by the Reynold's Number) on the resulting velocity and pressure distributions in the computational domain, plots of the pressure, and the x and y components of velocity were developed against the coordinate position (in global reference frame) along three sample lines of interest at an elapsed time of 6 seconds corresponding to what qualitatively appeared to be fully developed flow. In particular, after running the simulations for both the steady and unsteady flow configurations, it was observed that the most interesting flow properties were displayed around the entrance to the cavity along the left and right wall surfaces as it was along these surfaces that resulting pressure and velocity distributions could be tied to theoretical behavior of surfaces exposed to high-impact winds from tornadoes and hurricanes, a main real-world application under consideration in the project. In addition to developing interest in studying the flow properties along the two wall surfaces, an objective of analyzing the flow properties along the midsection of the cavity from the cavity's entrance to its bottom was also established with an intention of describing the flow penetration, and pressure gradient/depressurization of the cavity.

Re=10

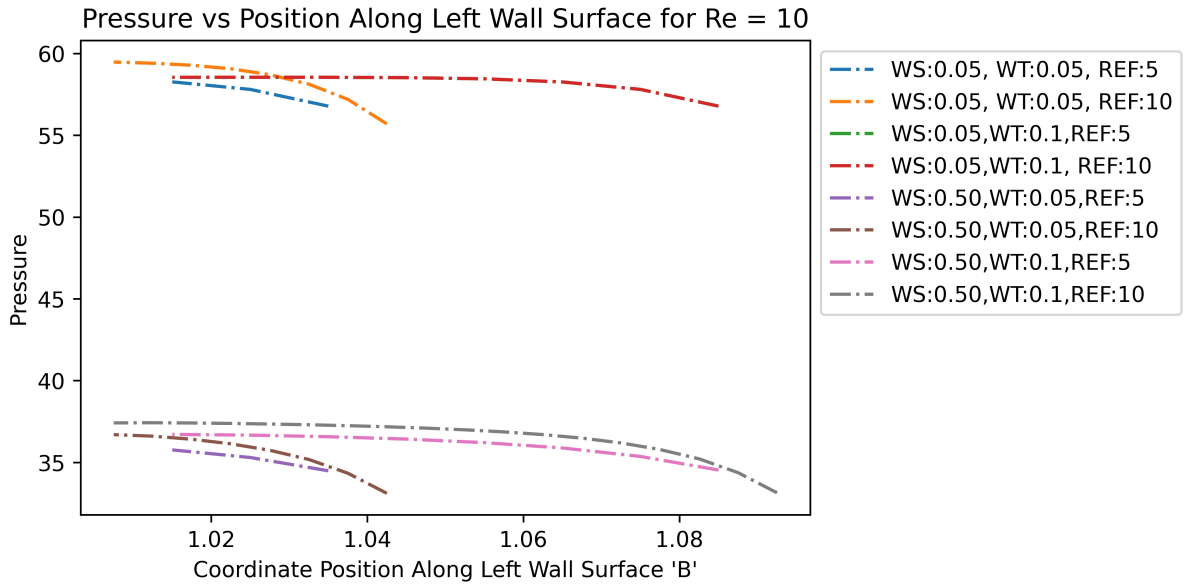

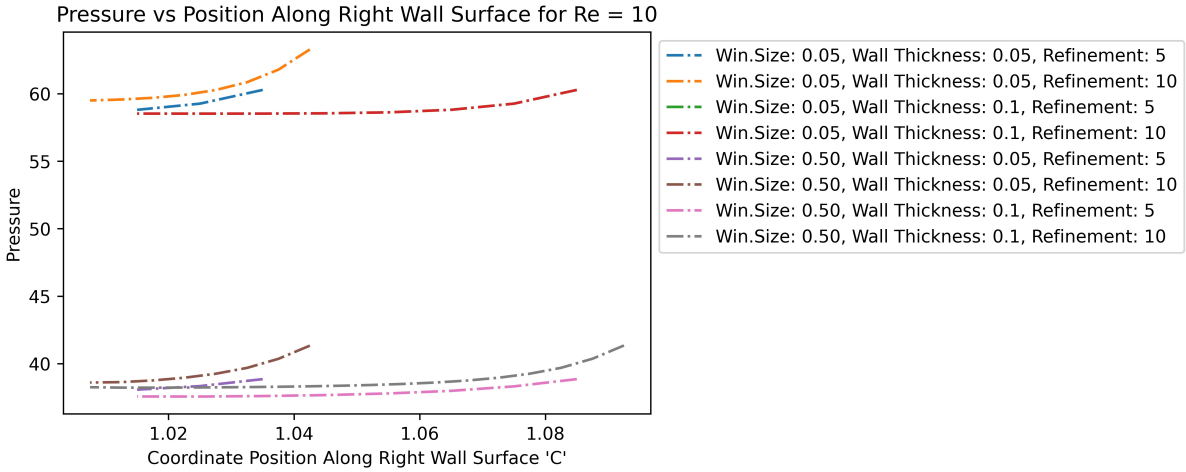

In examining the pressure vs position plot corresponding to the left wall surface flow for a Reynold's Number of 10, it can be observed the pressure decreases with position from the bottom of the wall to the top for all flow fields independent of mesh geometry and refinement. This agrees with theoretical behavior at an elapsed time of 6 seconds as by this the flow is fully developed and in steady state meaning flow along the left wall is moving from bottom to top as the recirculation region in the cavity tends to move clockwise and thus most of the flow leaving the cavity leaves along the left wall, and thus the flow along the left wall surface moves from an area of high to low pressure as the plot reflects. In examining the bottom four curves of the plot, it is shown that improving the mesh refinement increased the pressure across the wall for both of the window size-wall thickness pairs. Additionally, it is shown that as the wall thickness was doubled while the window size was held constant, the pressure across the wall surface increased as expected with more throughflow. Lastly, the flow fields from the simulations with a window size rescaled to 1/10 of the original value possessed a much higher range of pressure $[56, 59]$ compared to those from the simulations with a window size of 0.50 whose pressure range was approximately $[33, 37]$ as expected given that a smaller window size theoretically facilitates a greater amount of fluid build-up/pressure as the flow is more restrained. Shifting gears to the plot of the pressure vs position along the right wall surface, a trend similar to that shown in the previous figure is provided, namely, the pressure along the wall for mesh geometry with a window size of 0.50 and a fixed wall thickness of either 0.05 or 0.1 was about 2/3 of the value along the wall for mesh geometry with a window size of 0.05. Here, however, the pressure decreases from a maximum value at the top of the right wall to a minimum value at the bottom reflecting a region with a high pressure at the top and low pressure at the bottom.

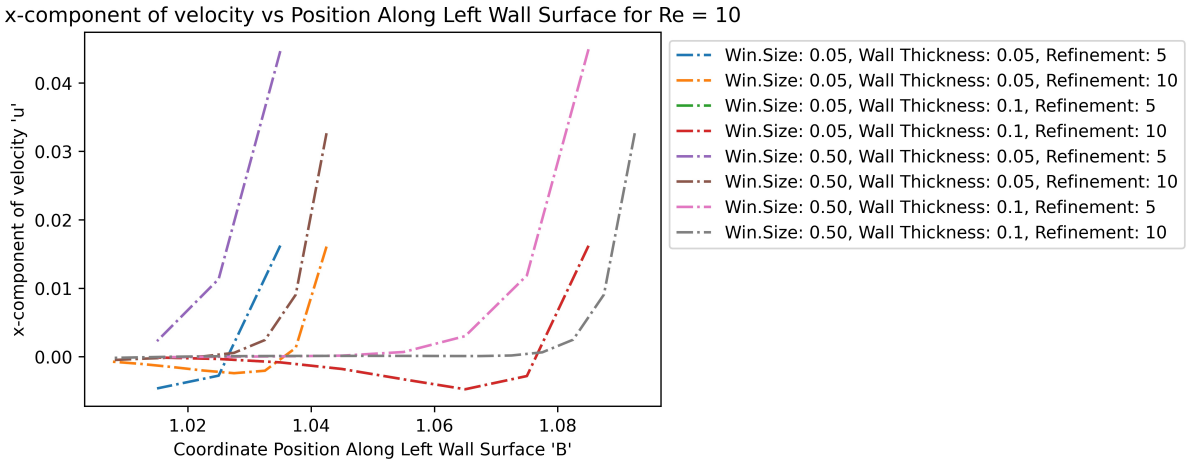

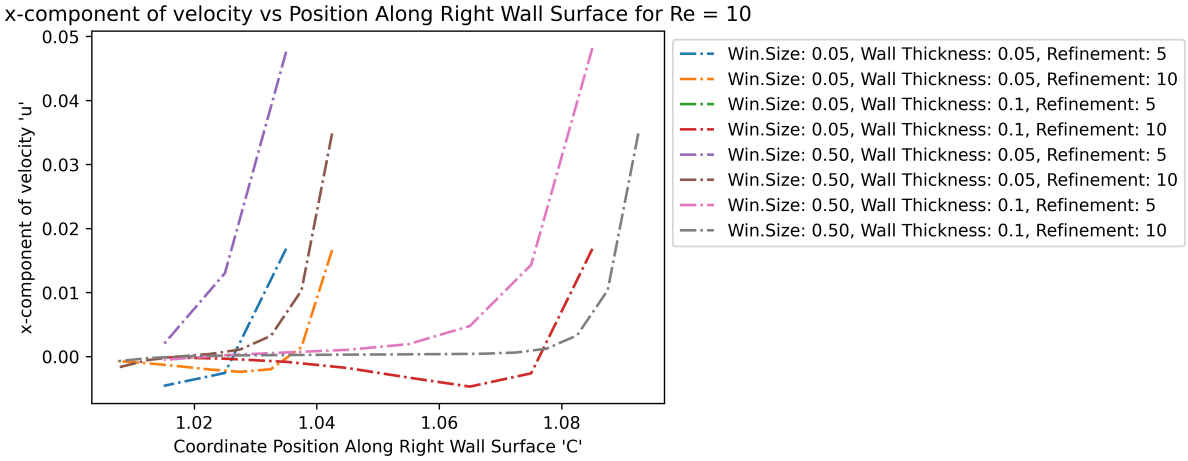

Shifting gears to the plots of the x component of the velocity across the left and right wall surfaces, it is shown that the curves are nearly identical whose features depict the velocity increasing slowly at first before finishing with a sharp increase in value at the top of the wall surfaces. This is reasonable given that the flow is at a maximum velocity at the inlet before before decaying in value as it moves further down the walls and ultimately, into the cavity. It is interesting to note that the simulations corresponding to the smallest window size and wall thickness produced velocity profiles that reached the smallest maximum value (~0.015) and decreased the most abruptly with position along the wall, whereas the simulations corresponding to the meshes with the largest window size and wall thickness decreased from the largest maximum value of the simulations (~0.047) very abruptly at the top of the wall before levelling off from around a vertical coordinate position of 1.06 downwards.

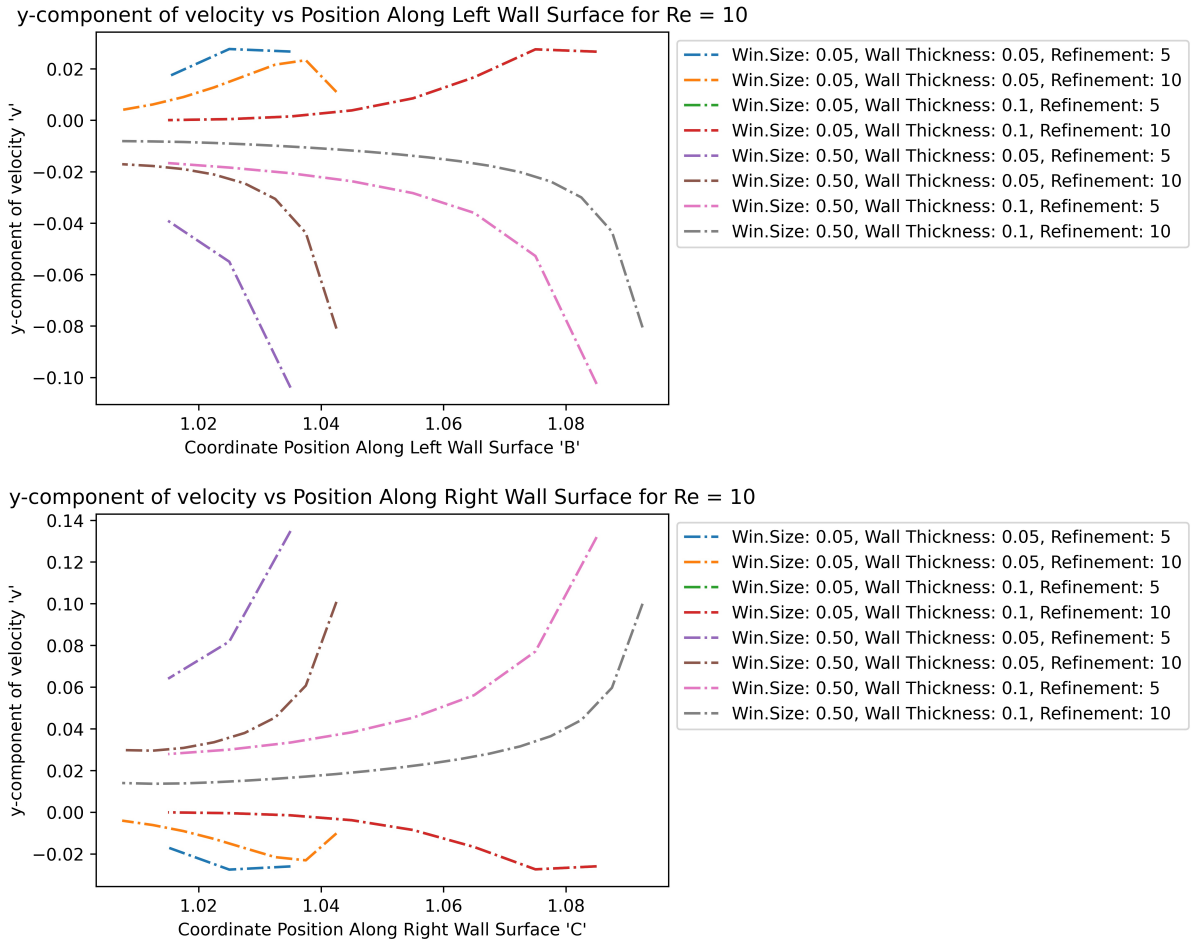

In examining the next two figures which depict the y-component of velocity as a function of position along the left and right wall surfaces, it is shown that they are a near mirror image of one another. Interestingly, the plot suggests that the y-component of the velocity in the flow fields corresponding to the simulations with a window size of 0.05 decrease from a slightly positive value to approximately zero from the top to the bottom of the wall whereas in the flow fields corresponding to the simulations with a window size of 0.5, the y-component of the velocity appears to increase relatively sharply from a large negative value at the top of the wall before levelling off at the bottom at a value that is slightly negative. The second figure depicts relationships that are suggestive of opposite features, namely, the y-component of the velocity from simulations with a window size of 0.50 dropped off sharply from a large positive value at the top of the right wall before levelling off at small and positive value at the bottom while values from the simulations with a window size of 0.05 increased gradually from a small and negative value at the top of the wall to approximately zero at the bottom. The reasoning for these reversed trends in the pairs of window sizes for both the x and y components of the velocity is likely attributed to the unsteadiness of the shed vortex and the effects from recirculation regions produced in the cavity whose properties impacted the flow along the surfaces. In general, it can be concluded that changing the wall size had a much larger effect on the pressure and velocity fields along the walls than changing the wall thickness.

Re=200

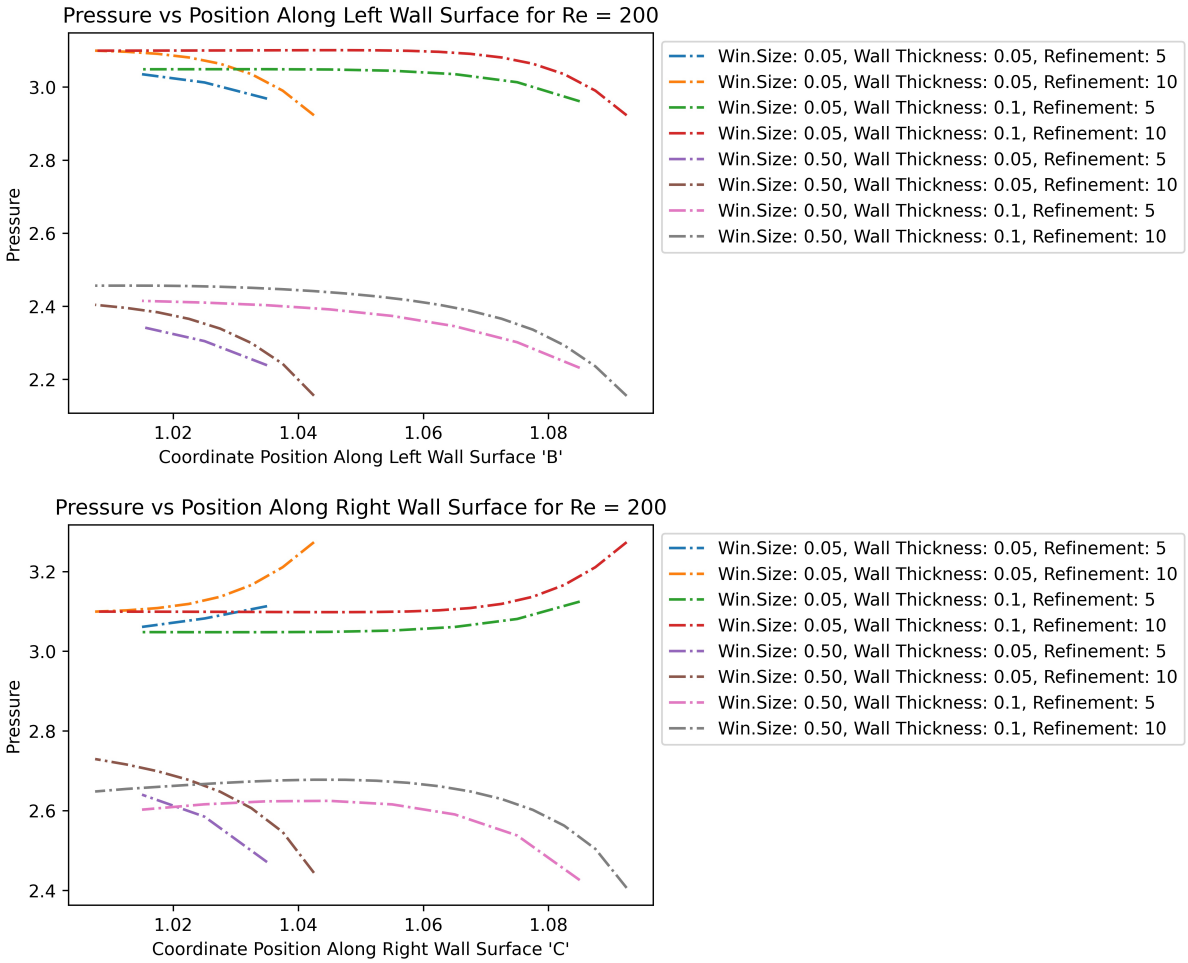

Shifting gears to the simulations run under a Reynolds' Number of 200, the flow fields remained steady, however, the shed vortex produced from the flow moving along the right wall and into the cavity split into four distinct vortices in the cavity that circulated clockwise over the cavity before ultimately being engulfed by the largest of the four and reaching steady state near the end of the simulations. As shown in the figures that depict the pressure fields across the two wall surfaces, the pressure again increased from a minimum value at the top of the left wall to a maximum value at the bottom, while the pressure decreased from a maximum value at the top of the right wall to a minimum value at the bottom. These high-low pressure regions are again consistent with the qualitative observations of the flow direction along the two surfaces. Interestingly, the pressure values for the Re $= 200$ simulations lie in the range $[2.1, 3.4]$, nearly a factor of 20 smaller than what was recorded for the Re $= 10$ simulations.

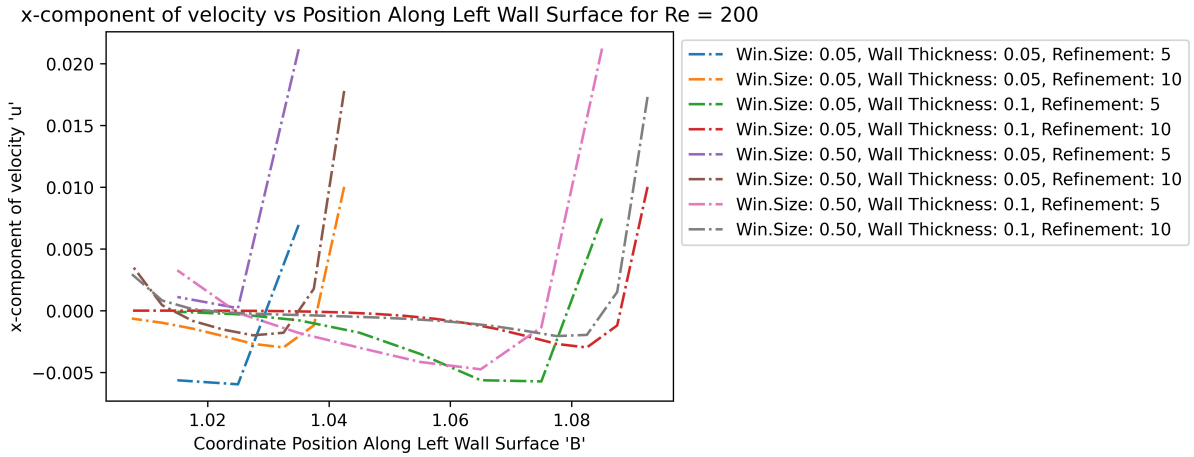

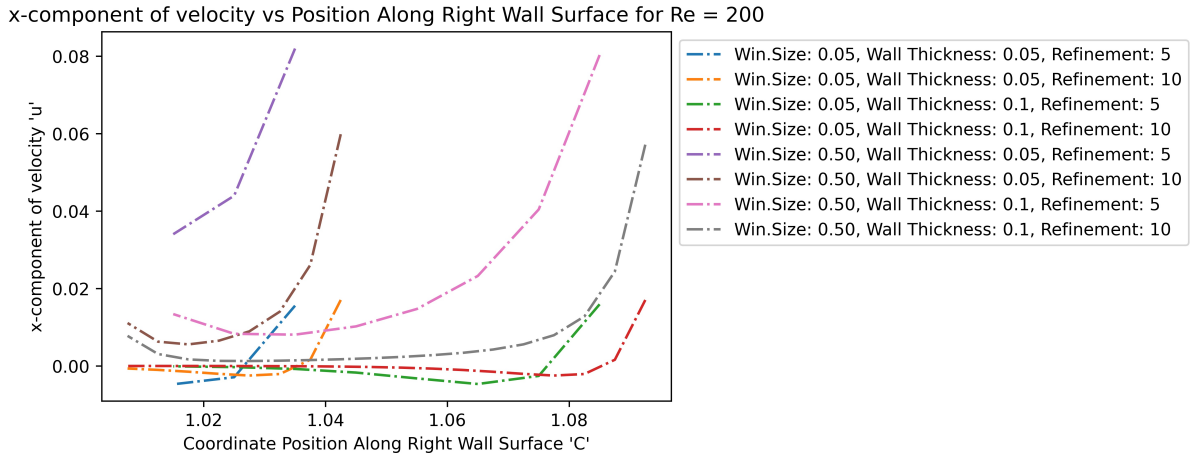

Looking now at the figures depicting x-component of velocity across the wall surfaces for Re = 200, it is shown that the x-velocity of the flow fields all drop off from a maximum value at the top-most point of their domain to an approximately minimum value near the bottom of the wall for both the left and right wall surfaces and independent of the wall thickness, wall size, and refinement parameters. These relationships are very similar to what was discussed earlier for the Re = 10 simulations.

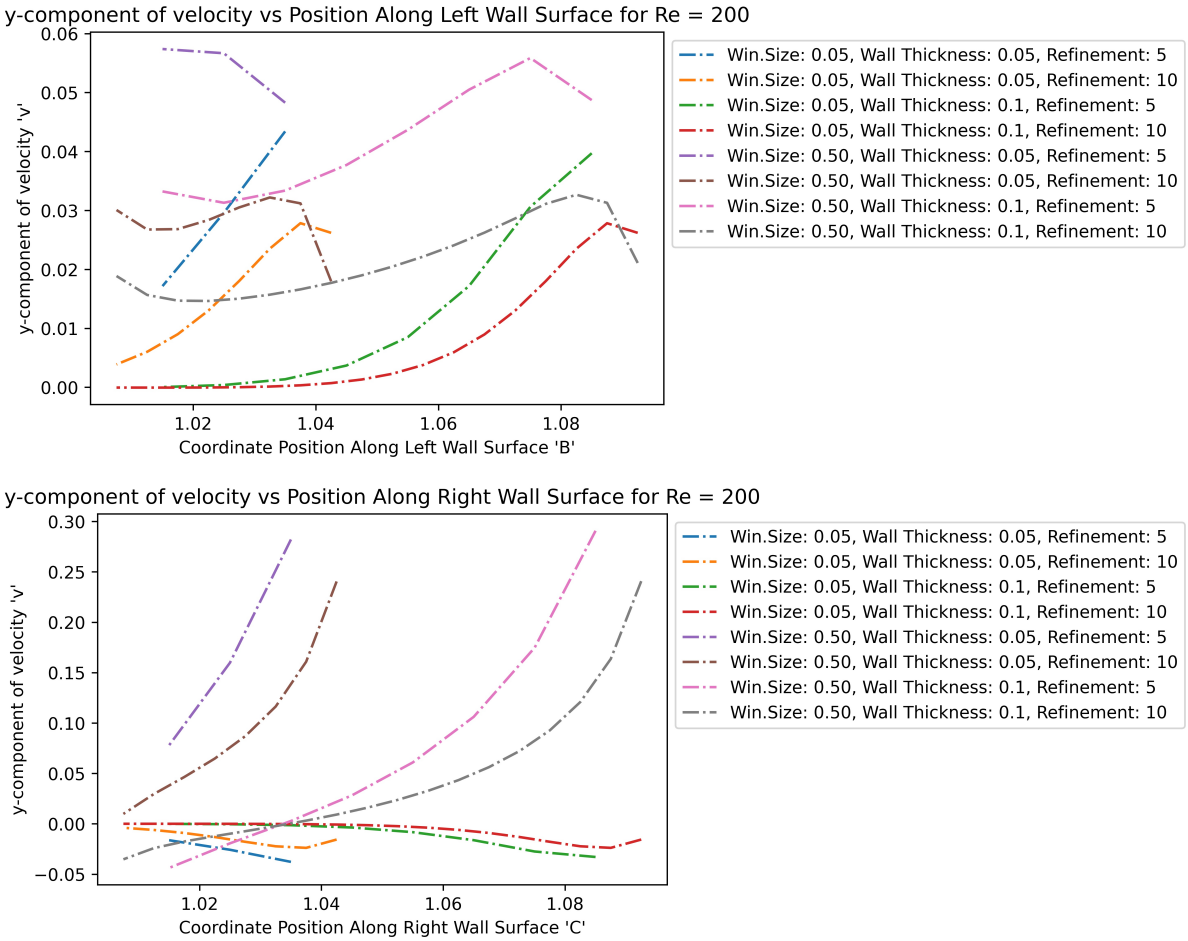

In looking at the plots of the y-component of the velocity along the left wall surface, it is shown that there is no distinct trend across the simulations run with a window size of 0.50, however, for the simulations run with a window size of 0.05, the values consistently decreased from a maximum value at the top of the wall to a minimum value at the bottom. Lastly, in observing the plot of the y-component of the velocity along the right wall surface, it is shown that for the simulations with a window size of 0.50, the values dropped from a maximum at the top of the wall to a minimum at the bottom whereas for the simulations with a window size of 0.05, the values marginally increased from a small and negative value to approximately zero as expected because for the simulations with a small window size of 0.05, very little flow penetrated the cavity along the right wall surface.

5.7. Cavity Midline Solution Profile

Now consider the profiles along the vertical midline down the cavity; from the middle of the window down to the back of the cavity.

Re=10

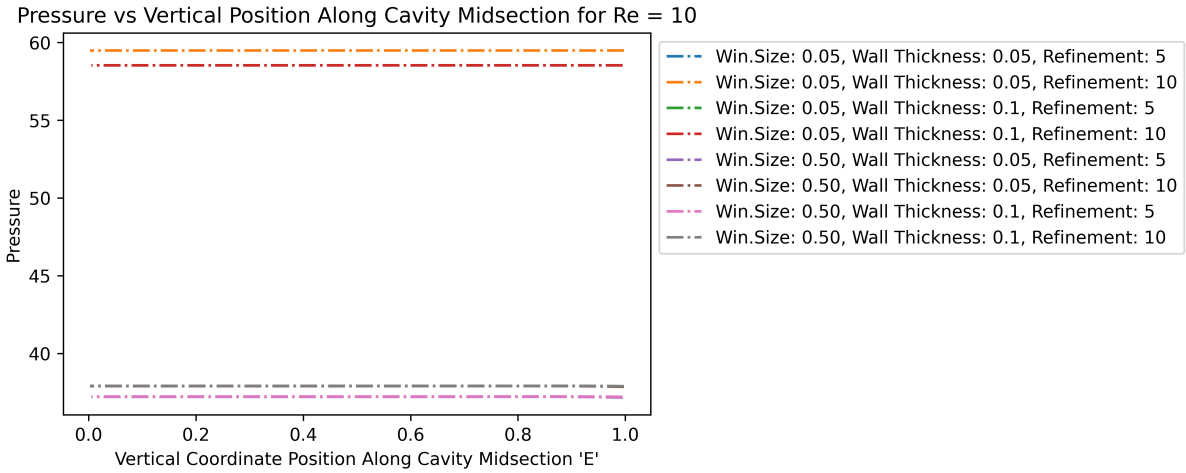

In examining the figure depicting the pressure across the cavity midsection for a Re = 10, it is shown that the distributions are constant with position for each combination of window size and wall thickness. The reasoning for the pressure distribution being constant over the cavity midsection is because of the symmetry of the flow for low Reynolds' Numbers and is a consequence of low pressure gradients across the low-speed centralized vortex that spans the midsection of the cavity such that there aren't measurably lower pressure values in the vortex center. Additionally, it is observed that for a fixed pair of window size-wall thickness combination, the relationship between pressure and position along the cavity is independent of the mesh refinement as evidenced by four curves overlayed onto four plots. Moreover, the simulations with the largest window size produced flow fields with the smallest constant pressure ([36,38]) compared to [58,59] which is reasonable considering that window size was determined to be inversely proportional to fluid pressure both along the wall surfaces and in the cavity from qualitative observations of the flow field generated from post-simulation movies.

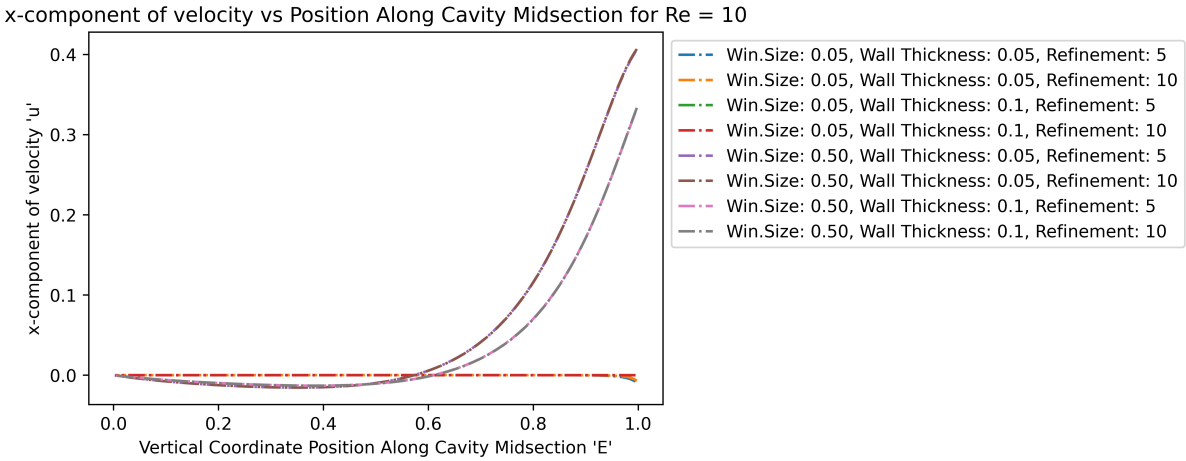

In observing the figure depicting the x-component of the velocity across the cavity midsection, it is shown that the simulations with a window size of 0.50 and wall thickness of 0.05, and the simulations with a window size of 0.50 and a wall thickness of 0.1 produced very similar x-velocity profiles where the values decreased sharply from a maximum value at the top of the cavity to a minimum value (approximately zero) at the bottom as expected. It can then be concluded that this trend was independent of the wall thickness. Interestingly enough, the mesh refinement did not impact the solutions, and thus, a focus in future work would be to explore increasing the resolution of the mesh even further. Another interesting thing to note is that the x-component of the velocity for the simulations with a window size of 0.05 remained constant across the cavity midsection likely attributed to low throughflow conditions under this geometry.

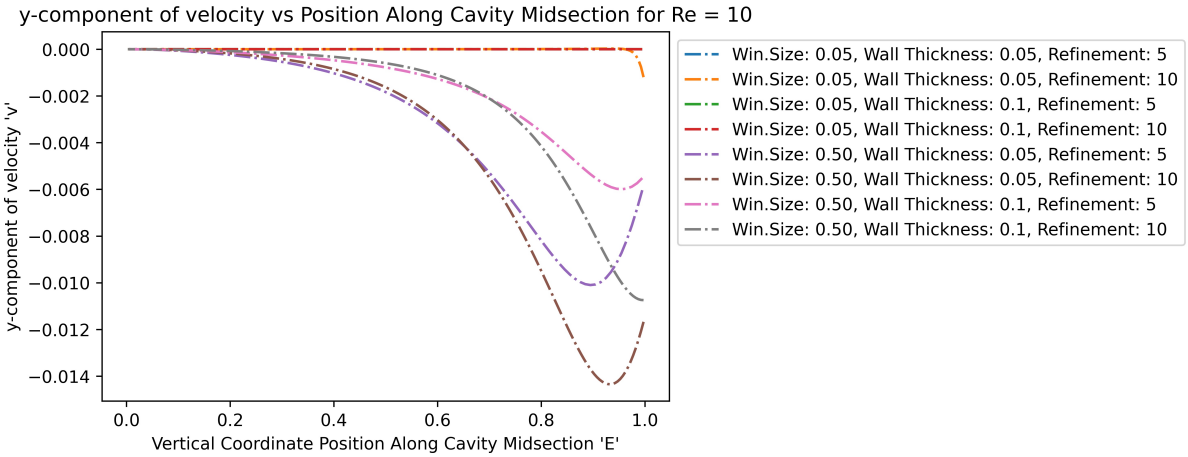

Transitioning to the plot of the y-component of the velocity across the cavity midsection, it is shown, similar to the x-component of velocity, that for a window size of 0.05 the values remained constant at approximately zero over the entire midsection again attributed to low throughflow for this geometry. Conversely, the results for the simulations with a window size of 0.50 suggest that the y-component of velocity dropped off in magnitude from an appreciably large negative value at the cavity entrance to roughly zero which is reasonable considering the larger observed throughflow from the simulation movies and given that less and less of the flow penetrates the cavity as the flow moves vertically downwards due to recirculation regions/vortices that are moving clockwise around the cavity.

Re=200

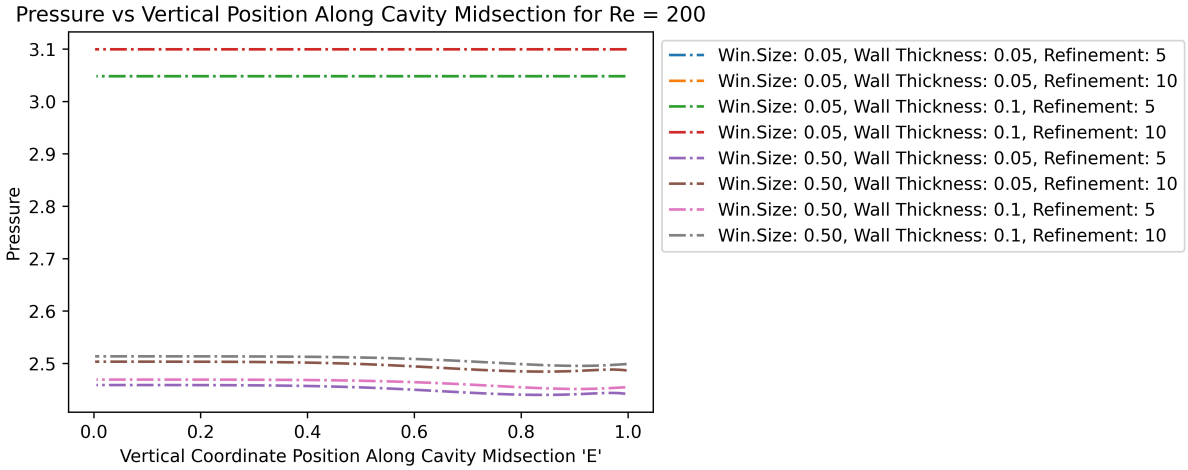

Transitioning to steady flow under Re = 200, it is observed in the first figure that the pressure distribution again remained constant across the cavity for a fixed window size-wall thickness geometry with the pressure magnitudes about a factor of 20 smaller than what was shown in the respective Re = 10 solutions. This agrees with the authors' intuition and expectations.

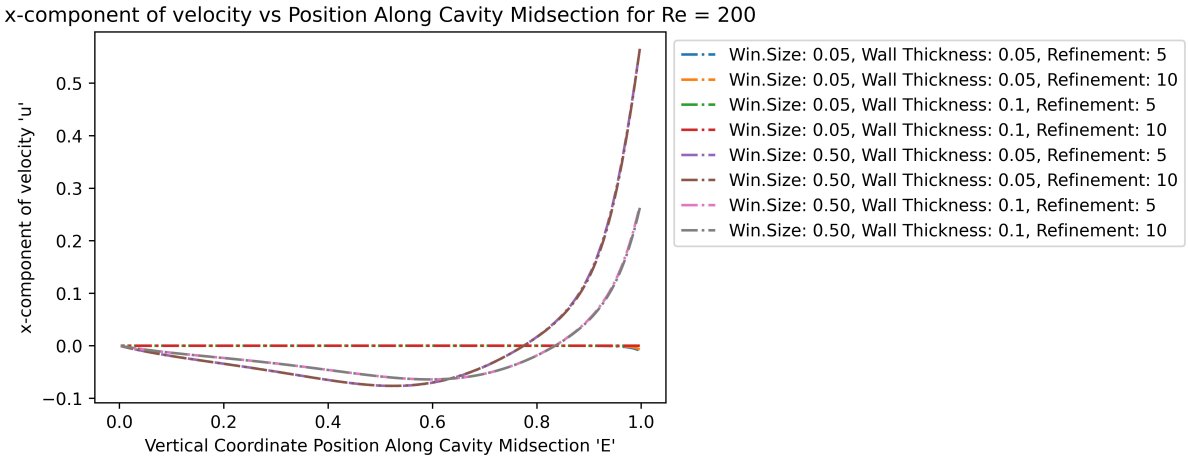

Shifting gears now to the plot depicting the x-component of the velocity along the cavity midsection, it is shown that the behavior is a near mirror image of the respective fields shown for the Re $= 10$ simulations, namely, the velocity drops off sharply from a maximum value at the top of the cavity's midsection before levelling off to zero near the bottom for the meshes with a window size of 0.50 and for those with a window size of 0.05, it remains constant at approximately zero.

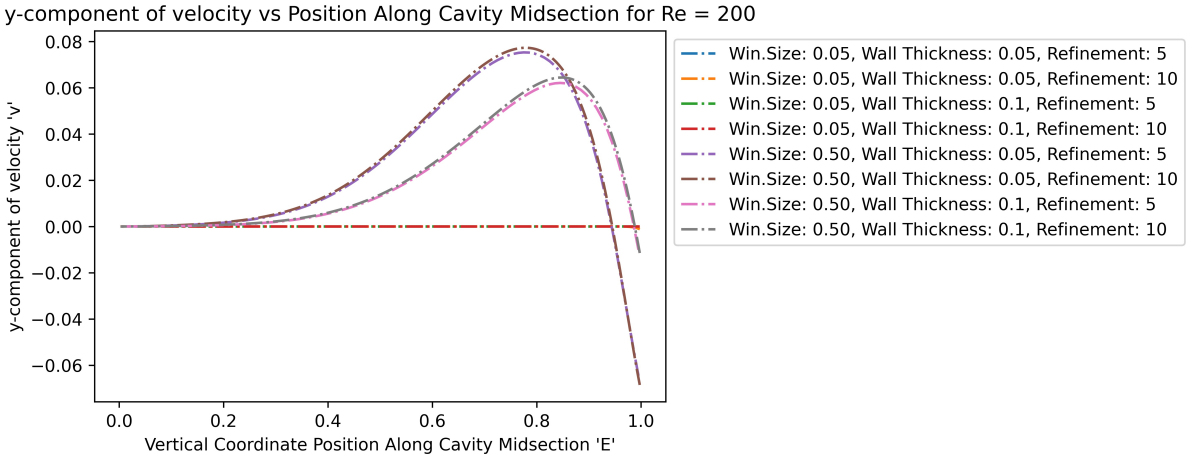

Interestingly, the figure above depicting the y-component of velocity across the midsection for a Re $= 200$ depicts relationships for the meshes with a window size of 0.50 that nearly resemble the solutions from Re $= 10$ reflected about the horizontal. In particular, the y-component of the velocity was shown to rising sharply from a large negative value at the top of the cavity before reaching a maximum positive value at a distance of roughly 0.2 into the cavity before dropping off again and levelling off to zero at the bottom of the cavity. This behavior is reasonable considering the effects of the centralized vortex in the cavity.

6. High Reynolds Number Part 1

Although low-speed Reynolds number flow is beneficial for primary flow analysis, the flow insuch a scenerio wold not prove catastrophic. Storms, be it hurricanes or tornados, contain flow of a high Reymolds number as is proportional to the velocity. In this section the flow behavior within a cavity of uniform wall thickness and window width will be analyzed with a high Reynolds number freestream flow outside of the cavity.

Note again all values are nondimensionalized - all lengths are in terms of L, the cavity length, all speeds in terms of U, the initial flow speed, and all times in terms of $\frac{L}{U}$.

The pressure is in terms of $\frac{p}{\rho U^2}$.

6.8. General Solution Form

Given the results from the Low Reynolds simulations, we will now consider only a window width of 0.5 and a wall thickness of 0.1. Images only for the refined mesh will be shown, for brevity.

Plots will be shown in the following order: P, U, UX, UY, P-contour, U-contour, UX-contour, UY-contour, Streamlines for T=60.

Re=1000

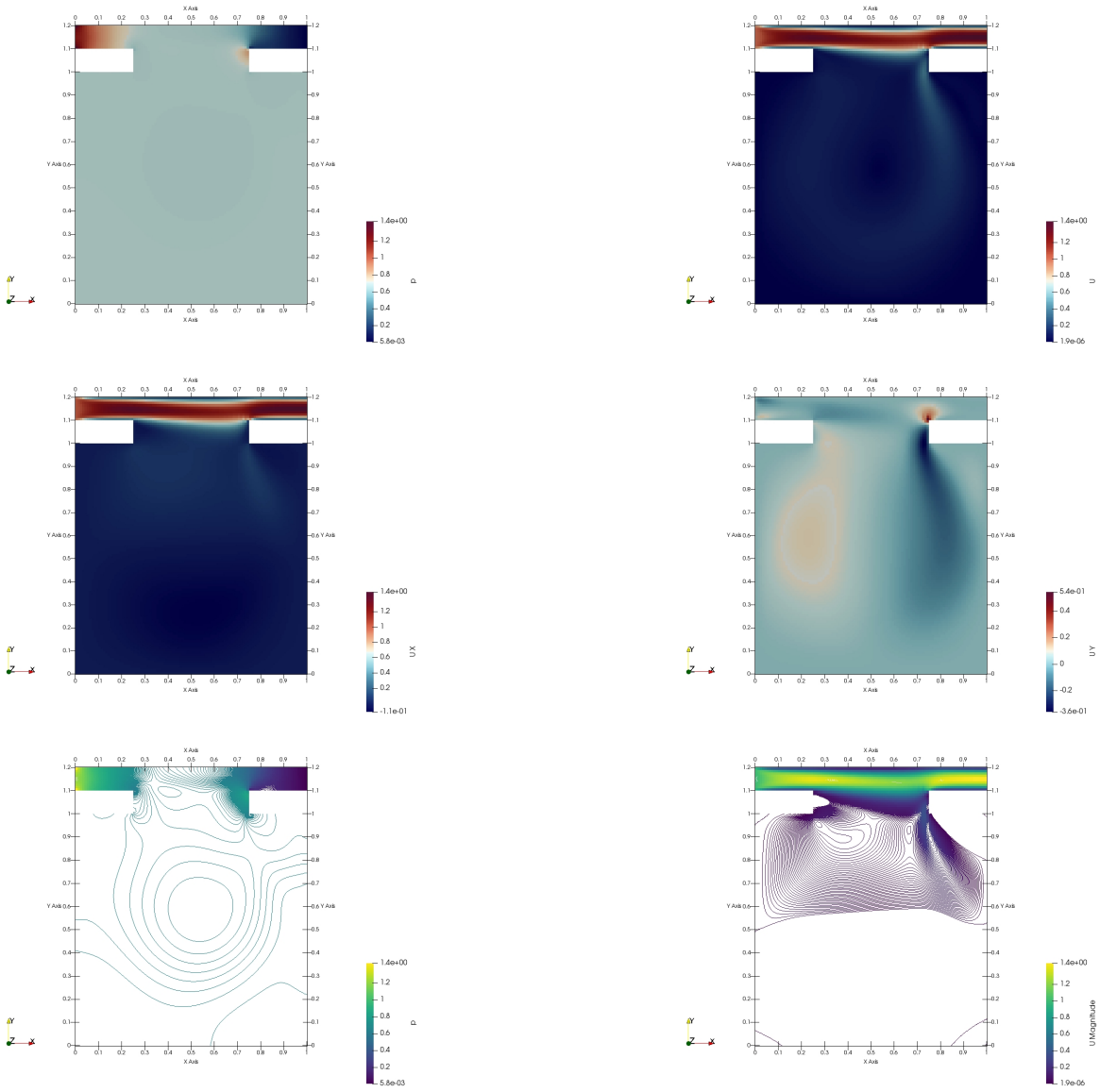

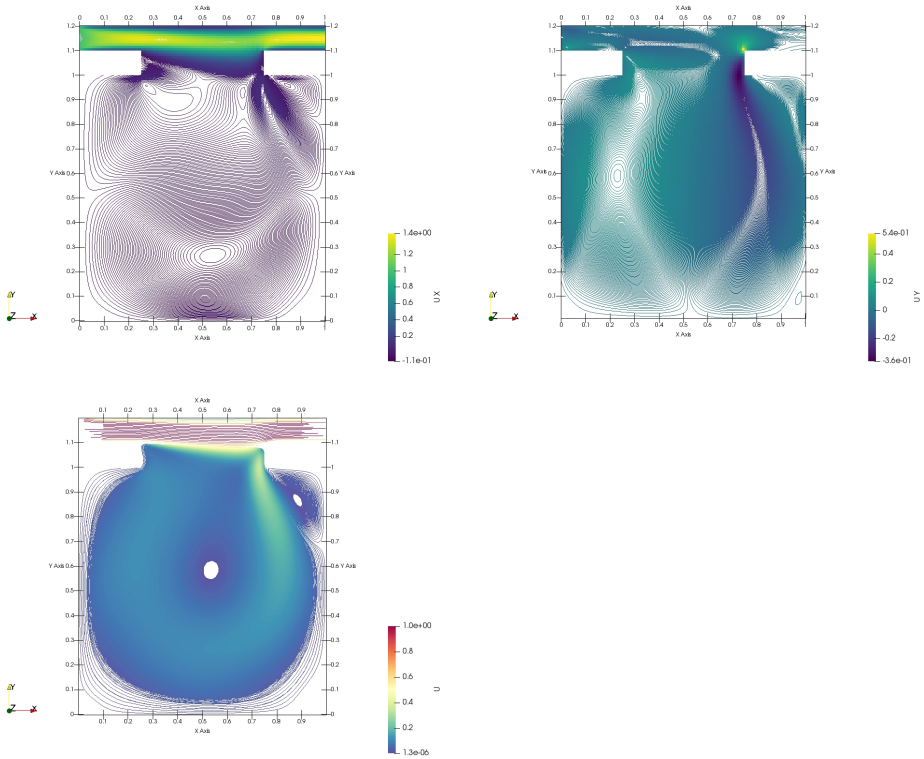

There is obvious vortex shedding at the right wall; one can see a tail extending into the cavity in nearly all the plots. Otherwise, this is quite similar to the low-Reynolds flow!
There is again a centralized vortice, an asymmetrical bend in the crossflow, and the hydraulic jump at the top of the right wall. The only difference is the tail, possibly a von Karman vortex street. To confirm that this is an unsteady flow, we look at the flow evolution over time.

Re=1000, U at T=1,2,6

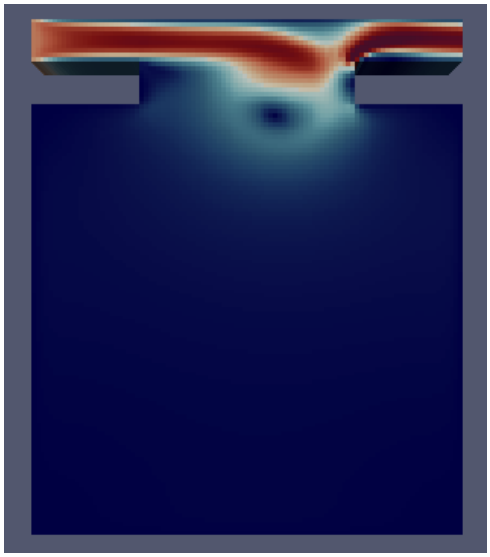

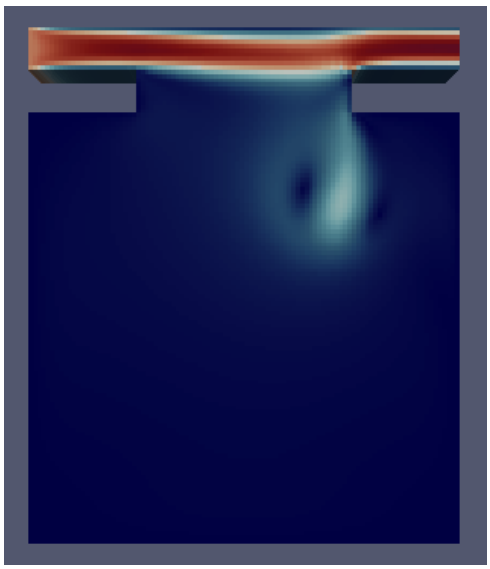

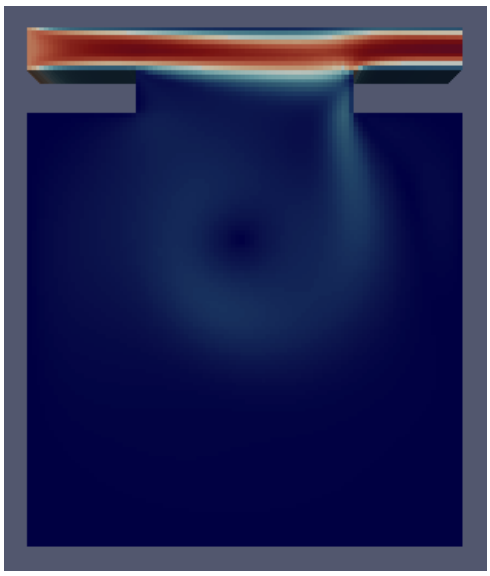

Clearly the flow is steady at large scales! So the vortex tail may not actually be a vortex street, since the unsteadiness is only at small scales. So Re=1000 is the above the lower-limit for the critical Reynolds number for large-scale flow, and below the critical Reynolds for small-scale flow. The overall critical Reynolds must then be between Re=200 and 1000.

Re=10000

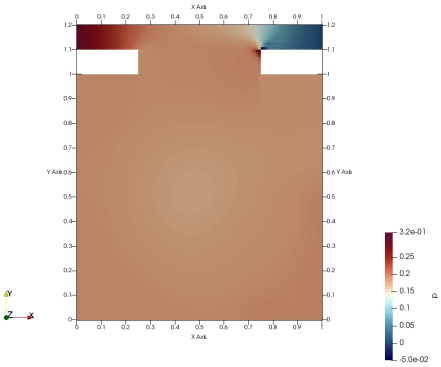
X Axis
Y Axis
3.2e-01
0.25
0.2
0.15
0.1
0.05
0
-5.0e-02
p

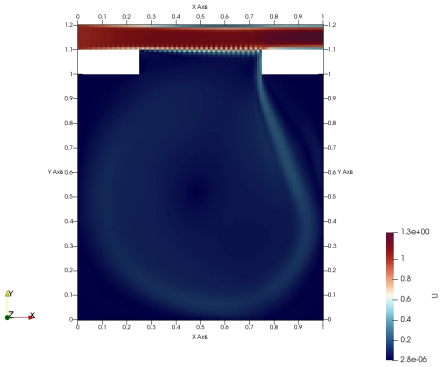
X Axis
Y Axis
1.3e+00
1
0.8
0.6
0.4
0.2
2.8e-06
U

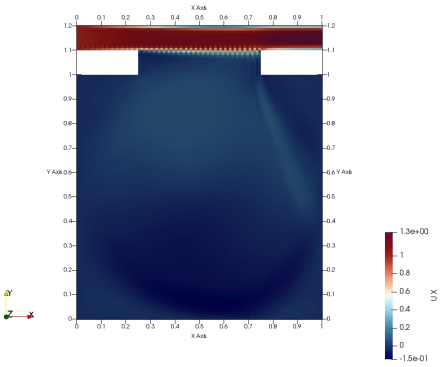
X Axis
Y Axis
1.3e+00
1
0.8
0.6
0.4
0.2
0
-1.5e-01
U:X

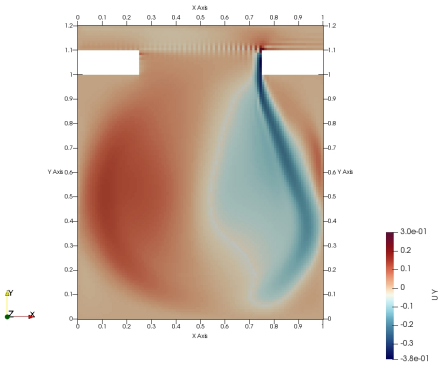
X Axis
Y Axis
3.0e-01
0.2
0.1
0
-0.1
-0.2
-0.3
-3.8e-01
U:Y

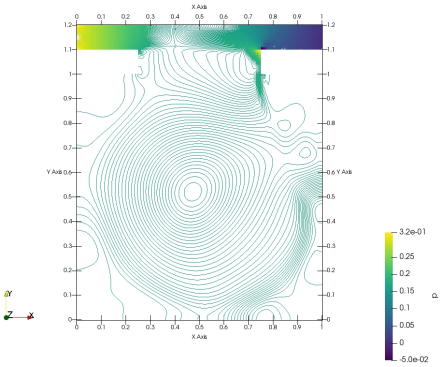
X Axis
Y Axis
3.2e-01
0.25
0.2
0.15
0.1
0.05
0
-5.0e-02
p

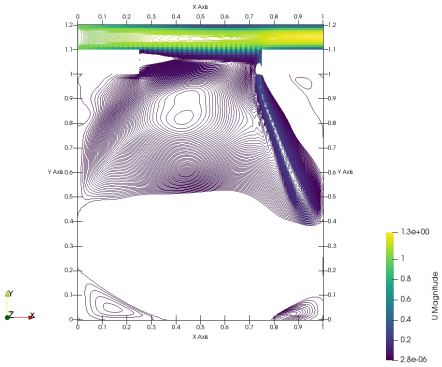
X Axis
Y Axis
1.3e+00
1
0.8
0.6
0.4
0.2
2.8e-06
U Magnitude

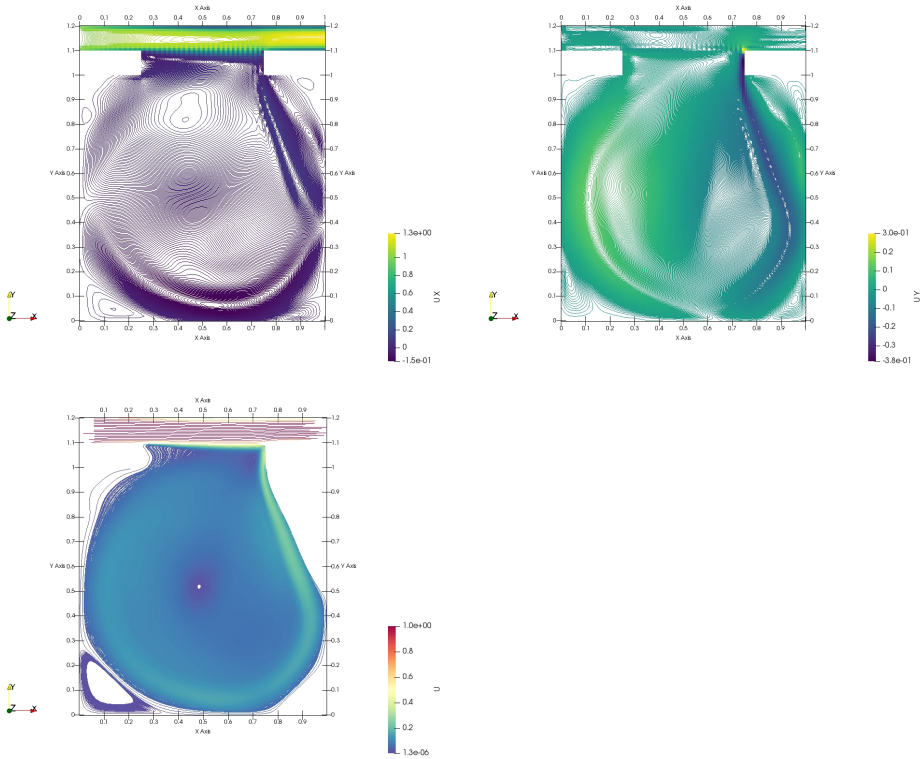

A much more well-defined vortex street can be seen here, and the only differences are really a more asymmetric flow with a stronger vortex street. This street can now be called such, since it does shed large-scale vortices, as seen in the following images over time. An important note: the vortex street originates from the hydraulic jump and propagates backwards, much like disturbances and sometimes turbulence can be seen behind a tidal bore or river rapids.

Re=10000, U at T=1,2,6,30

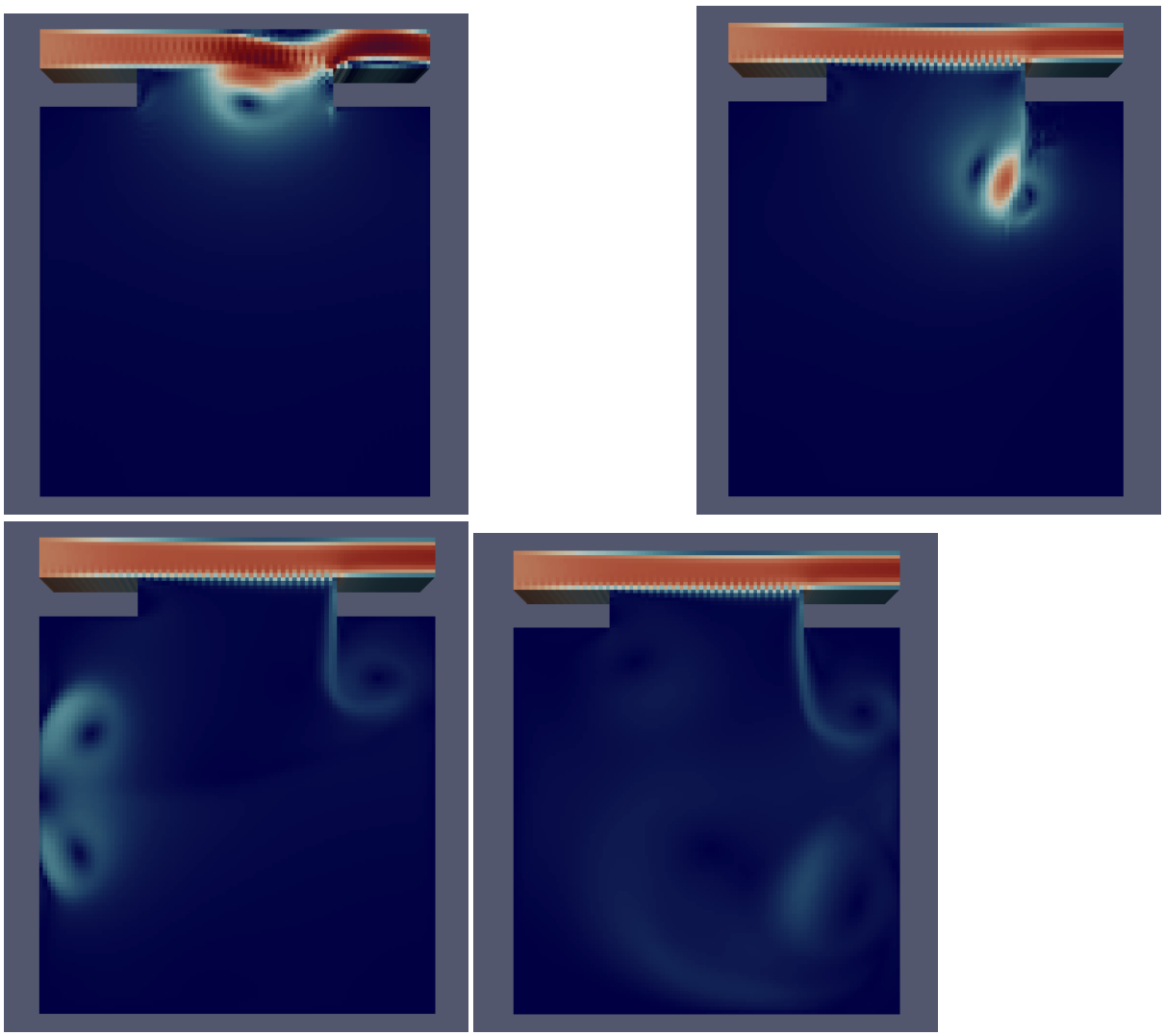

6.9. Vortice Positions

Convergence can again easily be seen by looking at the centralized vortex position for both meshes, by differing geometry.

meshfactor	Reynolds	window.a.	wall.w.	Vortex.Center.Location.along.Y
3	1000	0.5	1	0.691667
5	1000	50.0	1	0.705000
3	10000	0.5	1	0.641667
5	10000	50.0	1	0.595000

Table 5:

6.10. Strouhal Number and Vortex Shedding

The strouhal number is a dimensionless value that describes the behavior of flow oscillation. A very low Strouhal number denotes very few perturbations in the flow, whereas a very high Strouhal number denotes viscous behavior - while a moderate Strouhal number indicates vortex shedding.

We will now look at the frequency of the vortex shedding that occurs at the right window wall. In non-dimensional form (in terms of L/U), this is the Strouhal number. Two probes are placed 0.025 to the left and right of the right vertical wall, 0.05 below the lower

edge. We will denote the left probe as probe 0, and the right probe as probe 1.
Coarse meshes will be shown along with their refinements.

Fast Fourier Transform (over all time)

From the images shown earlier, clearly there is no vortex shedding for the Re=1000 case, and it seems to stabilize quickly, so one might assume that the flow is steady.
Below we have only treated the Re=10000 case, since the Re=1000 case does not produce useful filtered output (which might seem to corroborate the above.

Re=10000, Probe 0

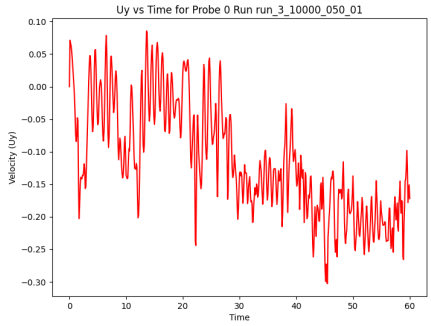

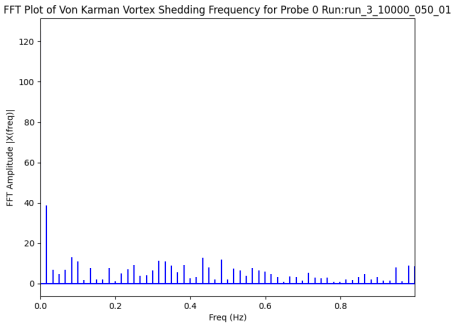

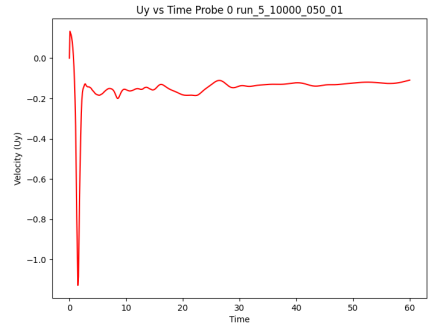

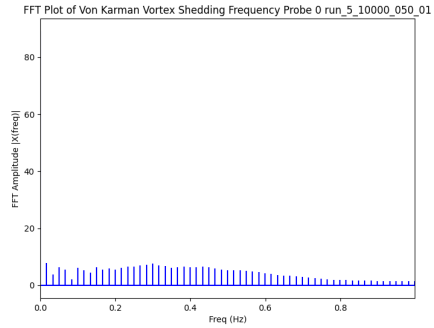

Re=10000, Probe 1

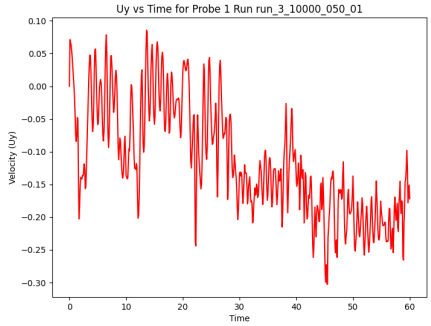

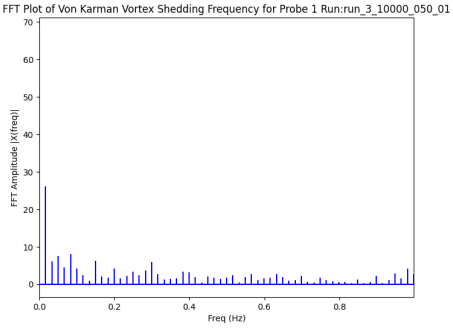

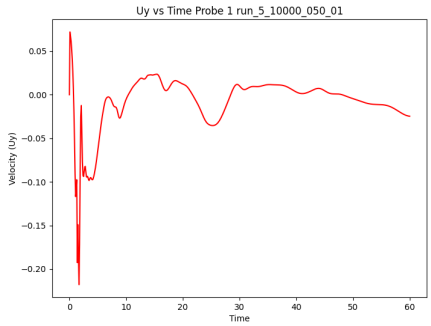

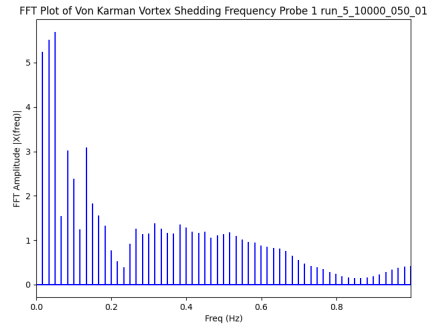

Note that the meshFactor of 3 fails to capture solution behavior (see the added oscillation).

Short Time Fourier Transform (spectrogram to see time evolution)

Re=1000, Probe 0

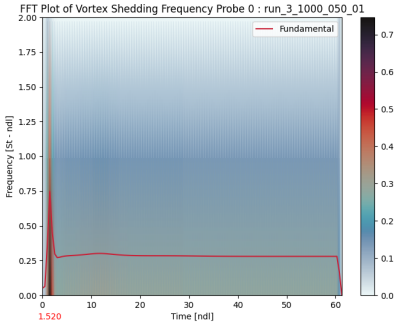

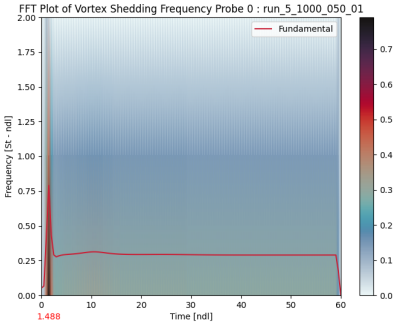

Re=1000, Probe 1

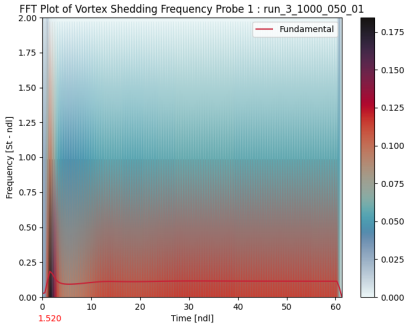

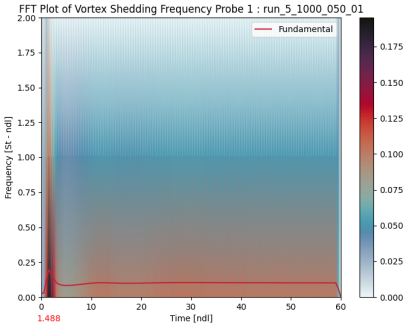

Interestingly, the Re=1000 plot is not at 0 Strouhal number! So we can clearly see that the large-scale flow does not have any steady-state oscillation (which is what the previous FFT plots show), but the small-scales are unsteady, with a typical Strouhal number near 0.2, as seen in the later table.

This is confirmed by the following:

> For spheres in uniform flow in the Reynolds number range of $8\times10\hat{}2 < \text{Re} < 2\times10\hat{}5$ there co-exist two values of the Strouhal number. The lower frequency is attributed to the large-scale instability of the wake, is independent of the Reynolds number Re and is approximately equal to 0.2. The higher-frequency Strouhal number is caused by small-scale instabilities from the separation of the shear layer.(Kim and Durbin 1988; Sakamoto and Haniu 1990)

Re=10000, Probe 0

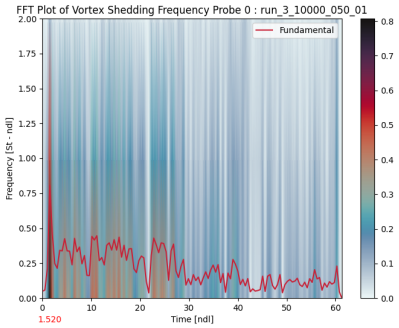

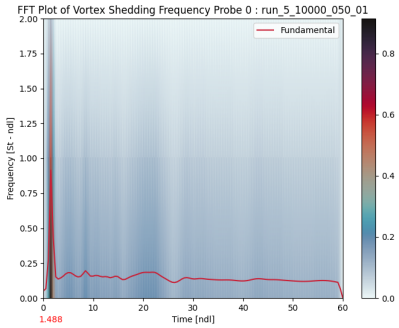

Re=10000, Probe 1

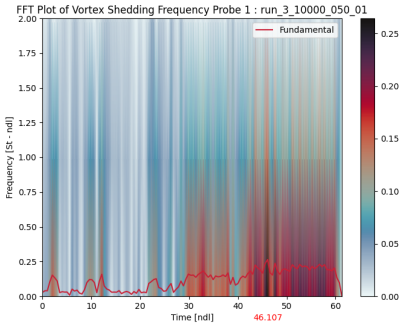

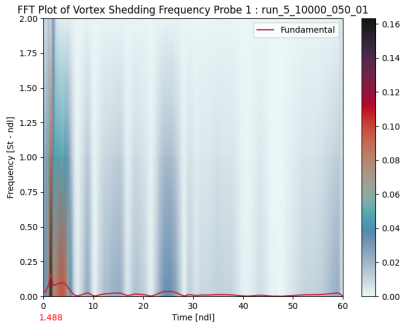

Continuing the former analysis, we see that the large scale instabilites are independent (since we get another Strouhal number for Re=10000 near 0.2 later in the flow). On the other hand, the small-scale instabilities are more prominent here, in the form of disturbances to the transform. We do not capture the other Strouhal number due to placement of the probes; we are interested in the large scale flow, so the other Strouhal number is not relavant for this paper.

Note again that the meshFactor of 3 is insufficient to capture the solution.

Equilibrium Large-Scale Strouhal Values

Note that transient Strouhal numbers exist for Re=1000, and there are also small-scale Strouhal numbers for Re=1000, but those are neither relavant nor easily retrievable for this study.

meshfactor	Reynolds	ProbeNumber	Strouhal
3	10000	0	0.116472
3	10000	1	0.166389
5	10000	0	0.316139
5	10000	1	0.149750

Table 6:

Note the stark difference between left and right frequencies - the higher one may be the second Strouhal number mentioned in the previously cited articles.

7. High Reynolds Number - Part 2

7.11. Window Wall Solution Profiles

Now consider again the profiles along the left and right window walls; the vertical segments along the inside of the window.
This time we will consider the starting behavior of these profiles at high Re, in particular between T=1 and 2.

T = 1.3 (unsteady startup)

Re=1000

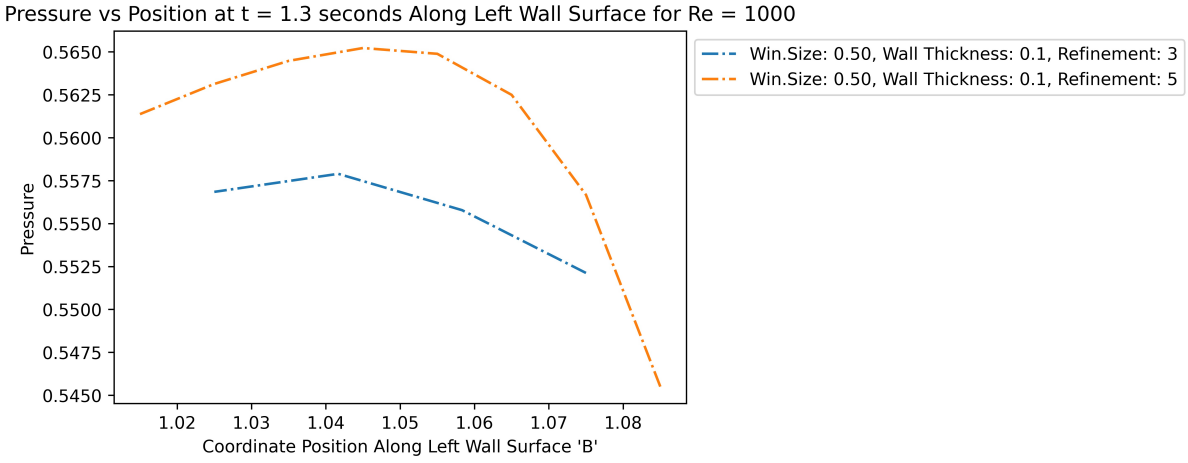

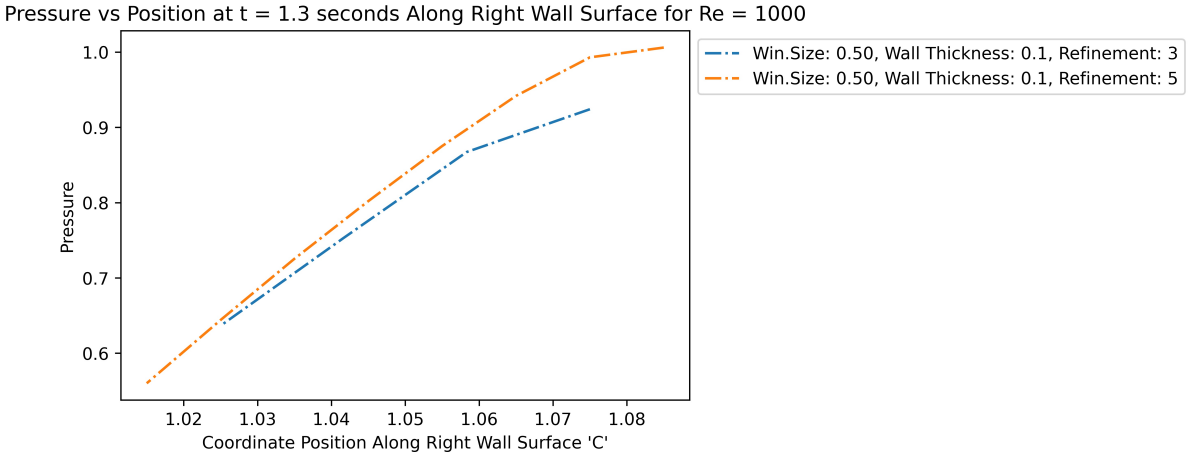

The pressure curves match the general images earlier; the only feature of note is the dip near 1.1, which is low pressure caused by rapidly accelerating corner flow.
The other dip at the cavity interior (near 1) is also due to the corner point; the lower velocity in the cavity compared to the crossflow causes the lower prominence of this dip.
By contrast, the right wall has a vortex just leaving the wall, so the sample is basically from the vortex center to edge, and we can see that the low-pressure zone caused by vortice is 0.5 ρU^2 lower than standard pressure.

Left Velocity

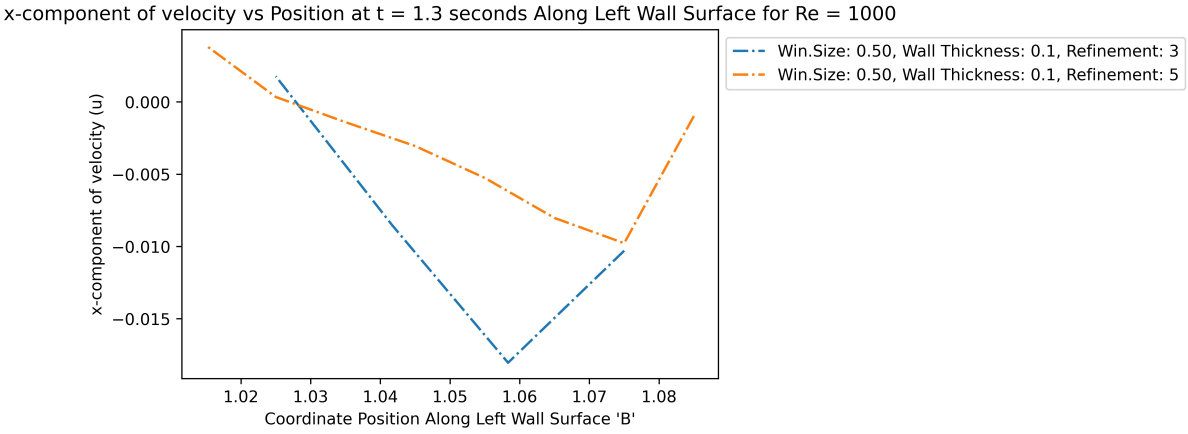

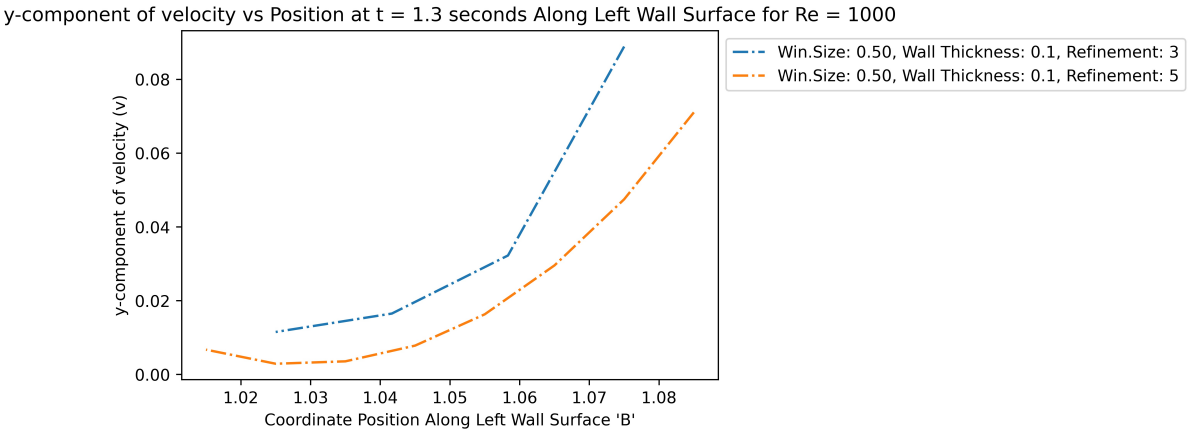

Important to note here is the stagnation point near the lower corner (at y=1.3). Both the X and Y velocities are 0 here. The flow above this point gets sucked back into the crossflow (as seen by the positive y-velocity and negative x-velocity) in a sort of recirculation, and the flow below this point remains in the cavity, moving up and right to join the part of the crossflow that enters the cavity.

Right Velocity

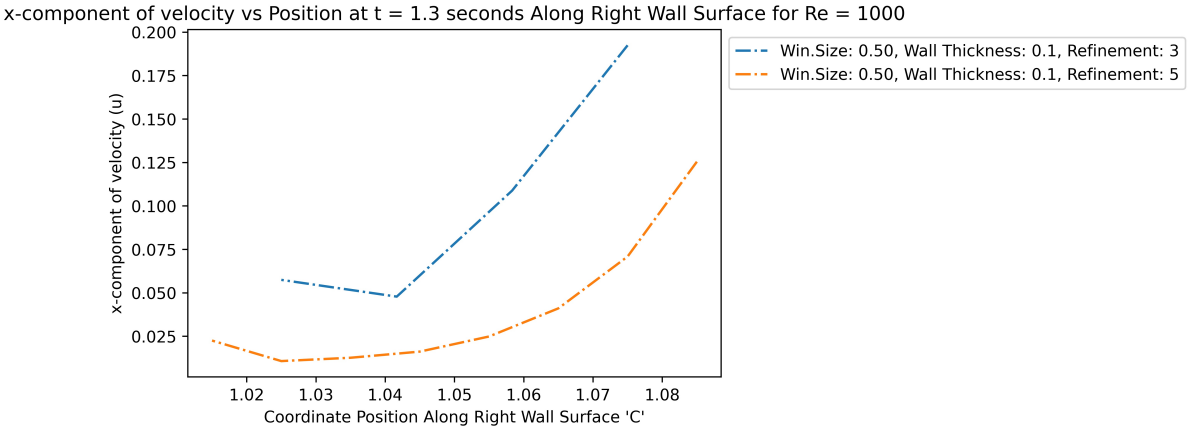

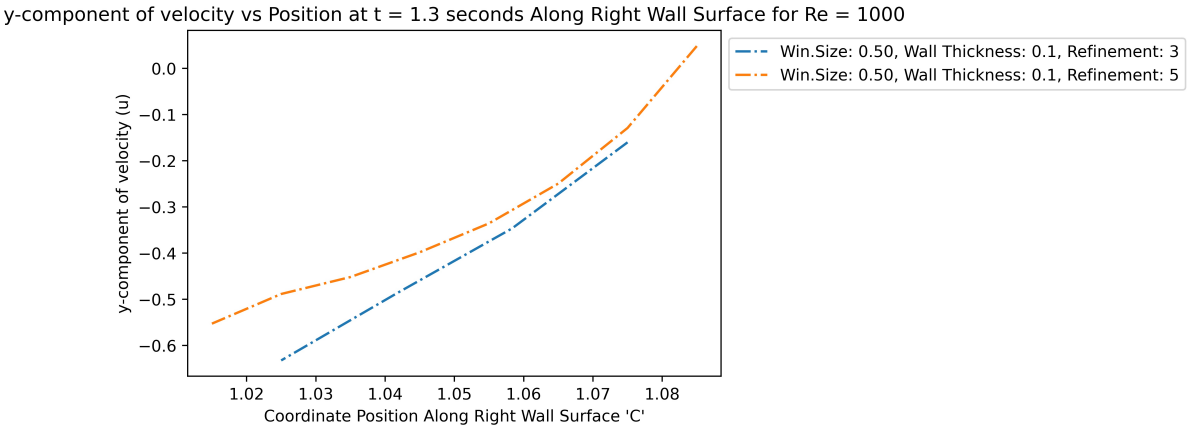

On the right wall, since we are sampling the edge of a vortice, the x-component is similar to 1/4 of a sinusoid (and this can be verified by noting from the earlier images that the vortice described here has a radius of approximatedly 0.1 (the wall width). The y-velocity is similarly sinusoidal, but has a strong negative velocity. Since we are almost sampling along the vortical radius, the velocity of the vortice wall should be roughly 0.6 U (free-stream velocity), and the vortex center (or eye) is moving downward at 0.6 U.

Re=10000

Since from previous results, we have invalidated the refinement / meshFactor 3 for Re=10000 as being insufficient, that will not be considered for convergence in the following plots.

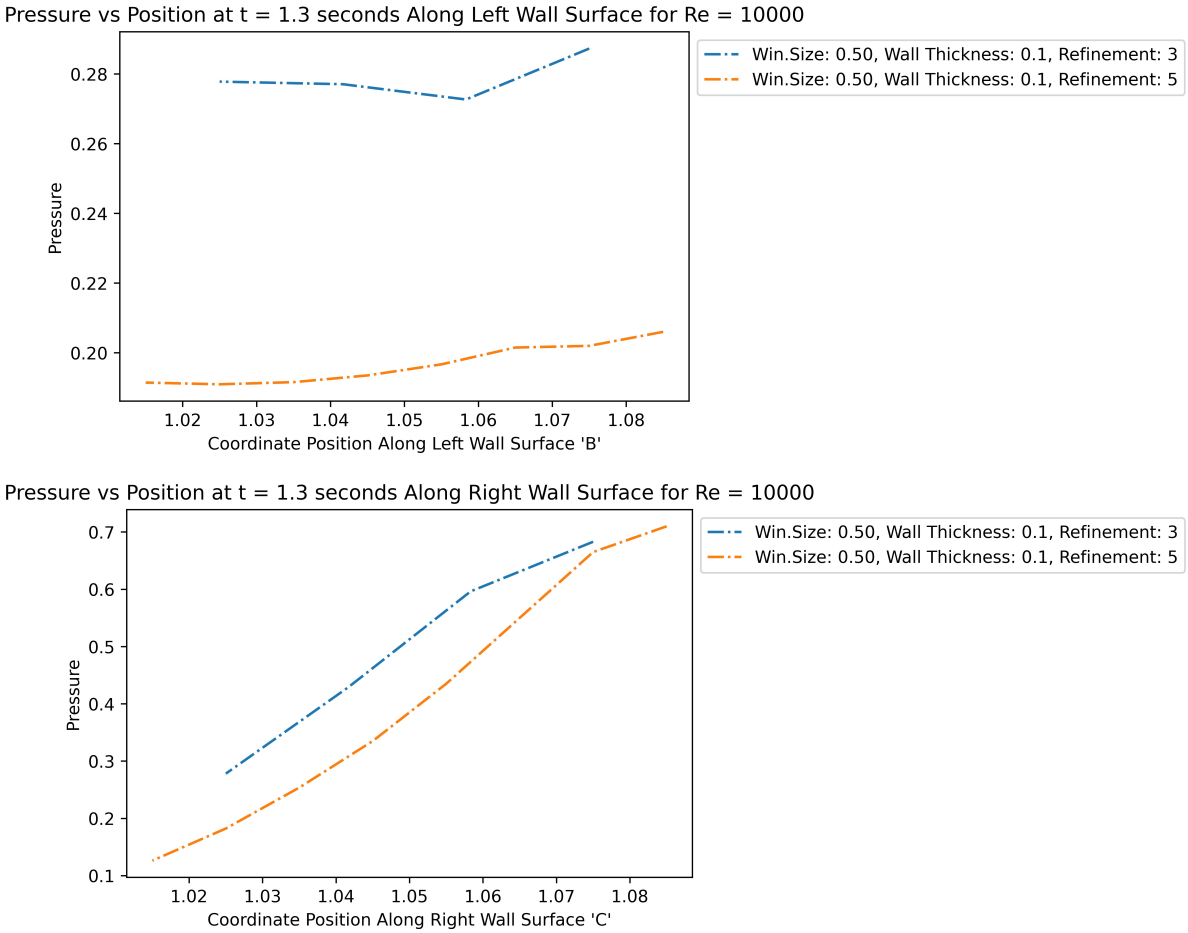

Just as before, the left wall has little to no pressure variation. Changing to Re=10000 has replaced the upper-left corner flow with a high-pressure region, possibly a stagnation point, implying that any inflow now travels further past the corner before moving into the cavity. Again, the right wall approximates the pressure differential across the main vortice, which seems to be about 0.65 ρU^2. Note the sharp corner in the fine-refinement pressure; that is probably the vortice edge.

Left Velocity

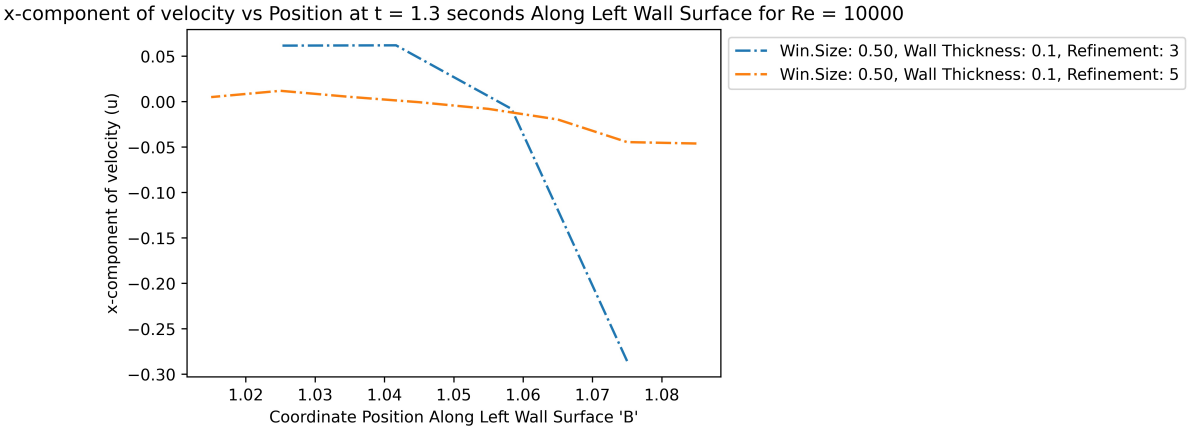

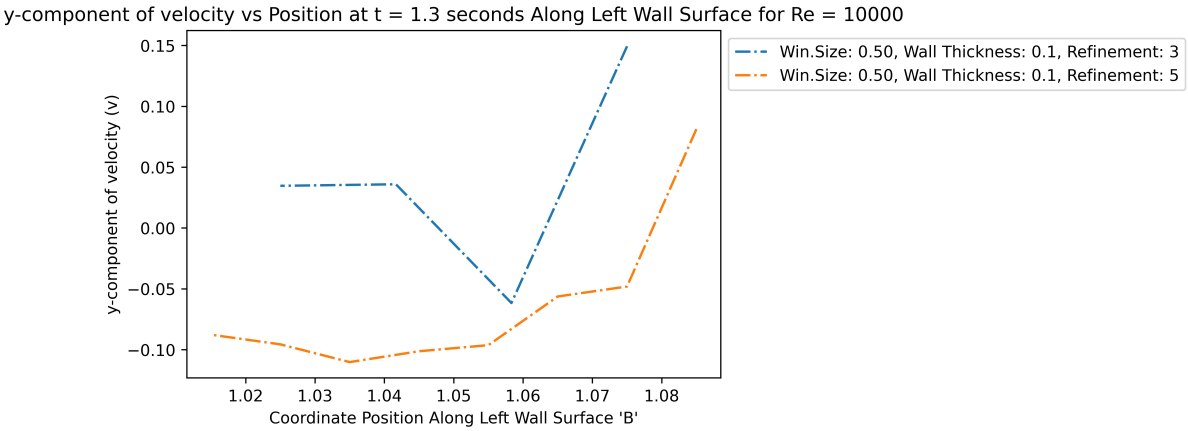

There is a really strong upward velocity with a negative x-component at the top-left corner, implying recirculation formation, which would correspond to the first transition vortice seen in low-Reynold flow. For the rest of the left wall, there is a small downward flow, possibly corresponding to the second transition vortice in low-Reynolds flow, again.

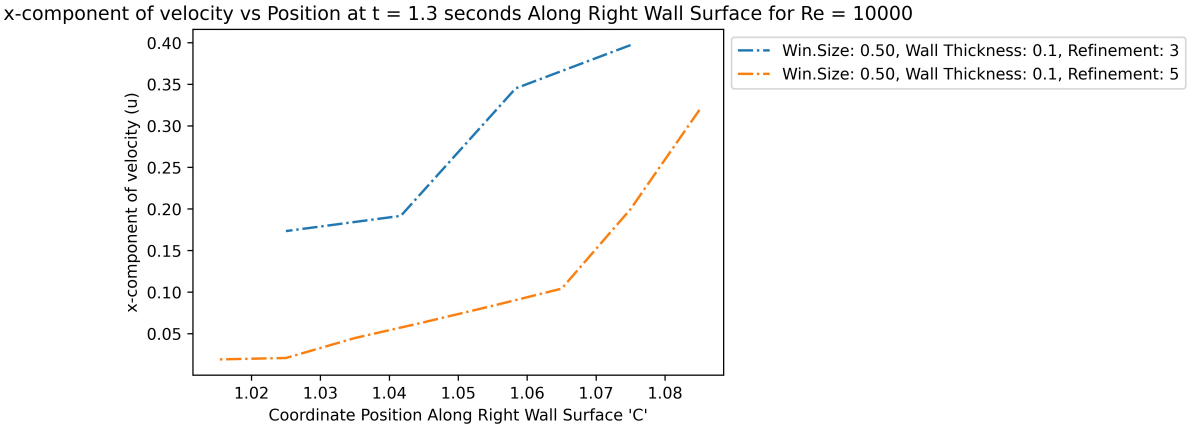

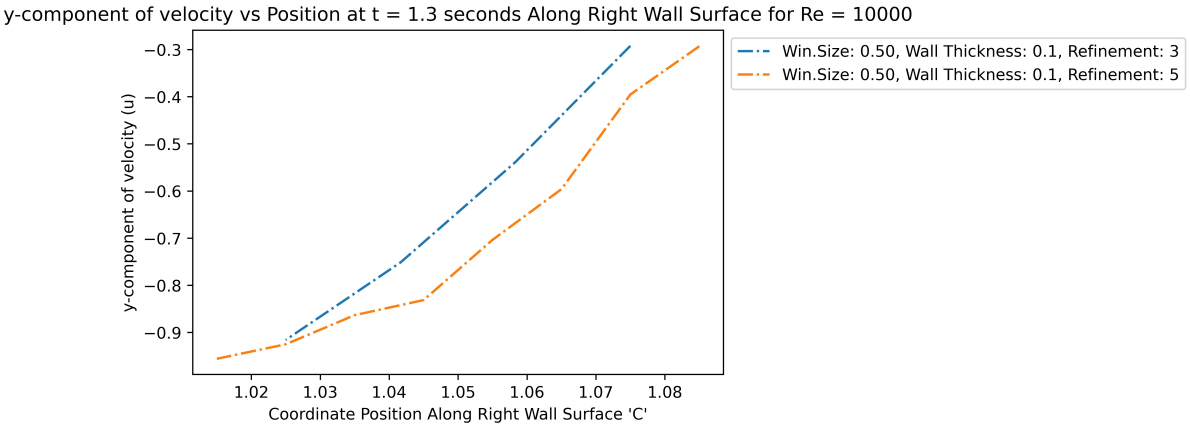

Again, from the images, this wall samples the main vortice. Looking at the X-velocity, and Y-velocity (stopping at the change in concavity), we see a difference in of about 0.3 and 0.6 ρU^2. So combining the speeds, the vortice speed (which will again be equal to rotation speed at edge) would approximately be about 0.67 ρU^2 (using L2 magnitude). Notice that this matches with the pressure in these non-dimensional units (since U=1), just like Re=1000, which is as expected.

Interestingly, most of the flow-field, with the exception of the vortex shedding, is identical to the low-Reynolds, which might imply that portion of the flow causes the Strouhal number of 0.2.

7.12. Cavity Midline Solution Profile

Now again consider the profiles along the vertical midline down the cavity; from the middle of the window down to the back of the cavity.
Similarly, we will only consider T=1.3.

Re=1000

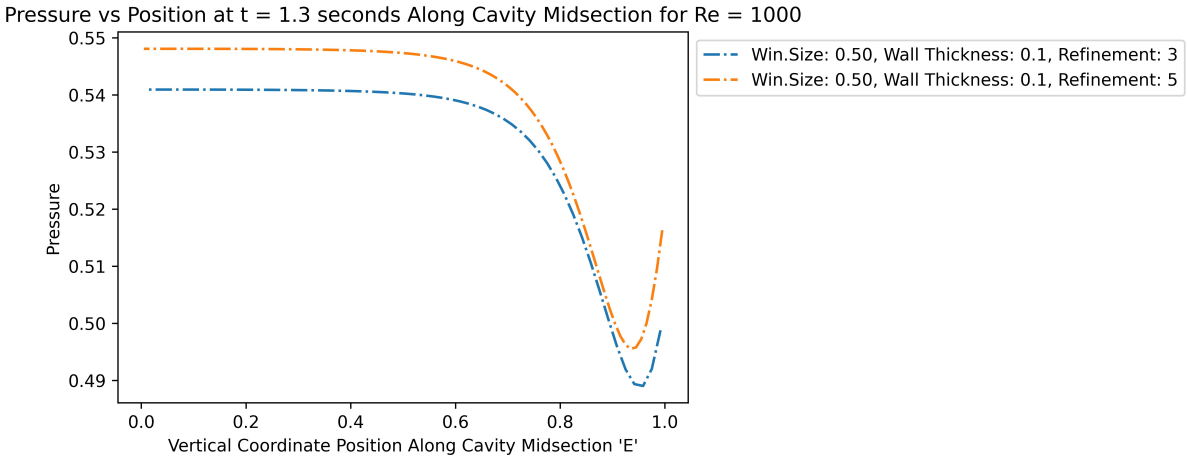

These profiles are fairly self-explanatory: the cavity pressure is constant as in the initial conditions, and just near the top, where the high-speed free stream enters, there is a localized low-pressure region due to the main vortice edge (since it is near the right wall at that time). This can be confirmed by comparing with the low-Re simulations; there is only relatively constant pressure for the low-Re flow!

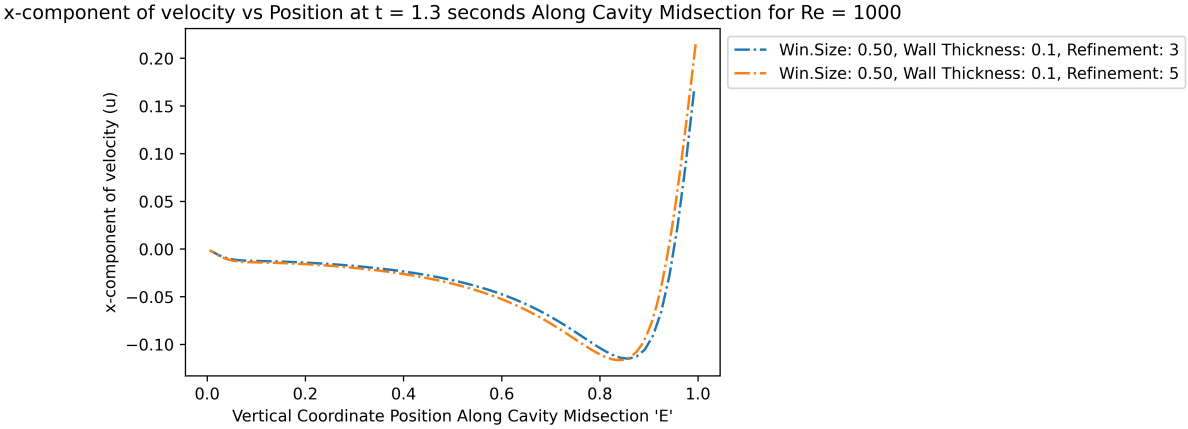

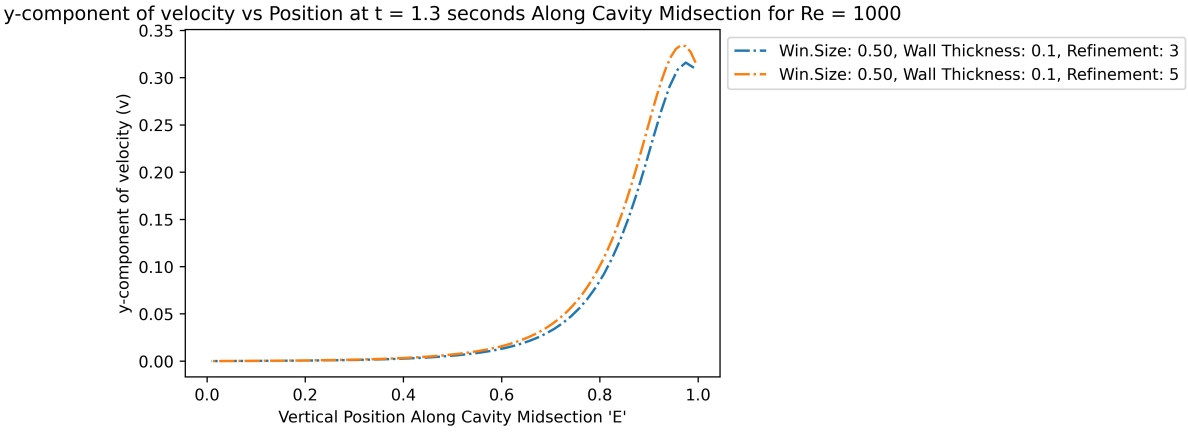

The X and Y-velocites corroborates. There is a much narrower range for the same features when compared to the low-Re simulations, and this is due to the vortice concentrating those features.

Note the amount of similarity from the low-Re plots!

Re=10000

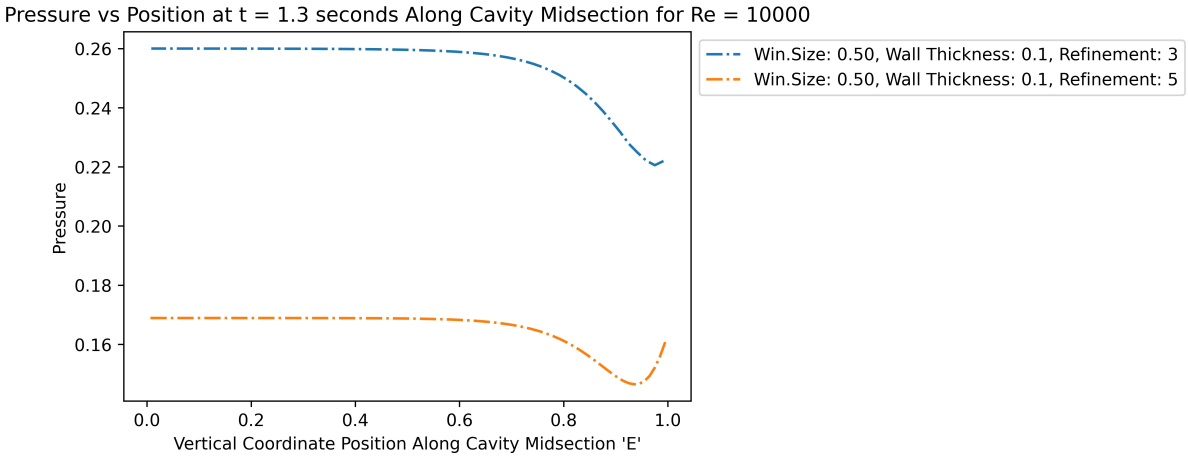

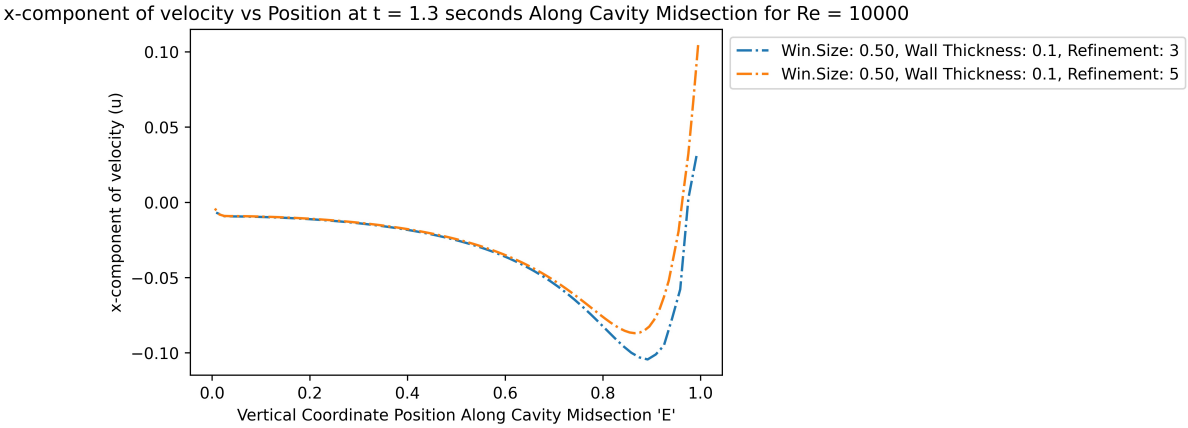

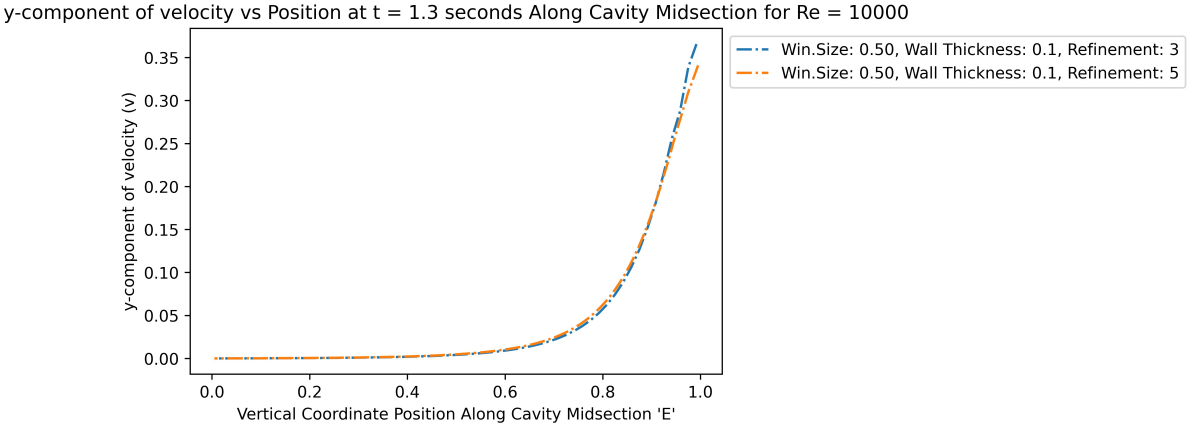

Comparing these to the Re=1000 plots, note that these plots are near identical, which implies that this large-scale flow measured along the cavity midline must correspond to the Strouhal number near 0.2, which is Reynolds-independent, explaining why the low-Reynold plots are so similar. Interestingly, despite the vortex velocity being reasonably larger than that of Re=1000, there is almost no difference in the plots!.

Mean Strain Rate over Time

Now returning to strain rate, to confirm that the maximum strain rate does occur at T=1.3, we plot the mean strain rate over time, for the left and right vertical window walls.

Re=1000

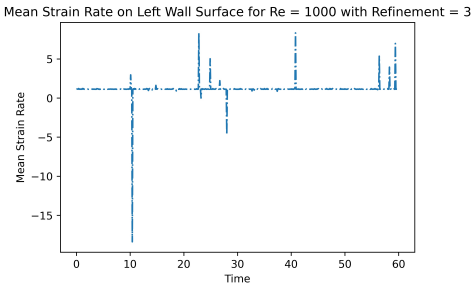

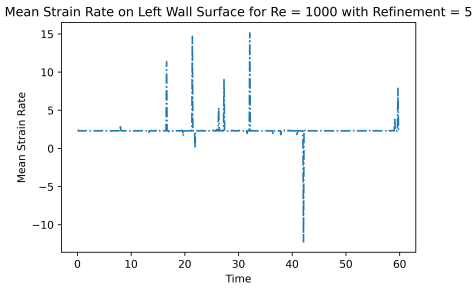

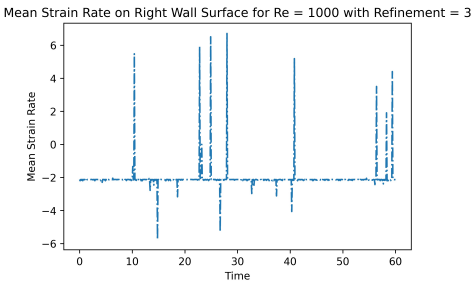

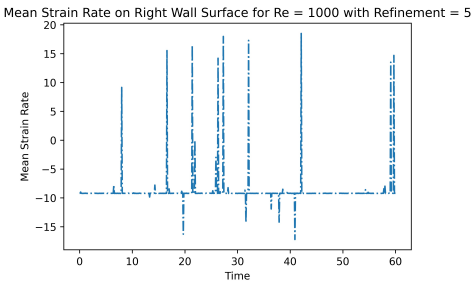

Re=10000

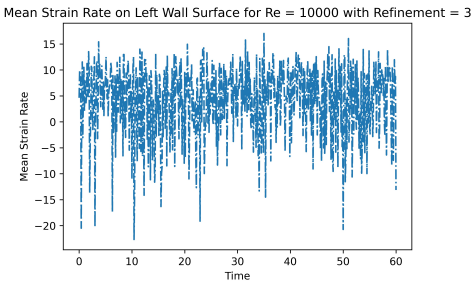

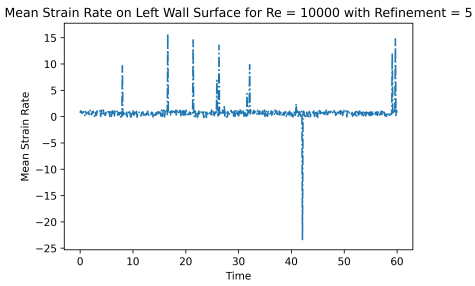

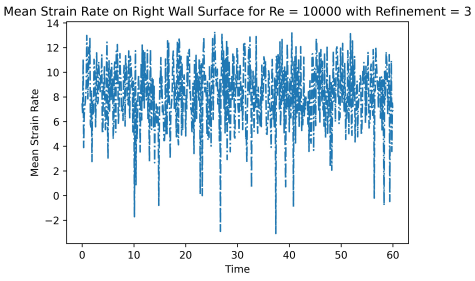

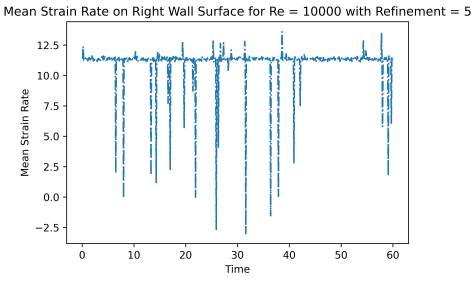

Unfortunately, these results do not match T=1.3 as maximum. Noting that the refinement or meshFactor 3 still fails for Re=10000 in a manner similar to the previous plots, we can probably rule out code errors. The possible other issues might be a lack of sufficient refinement, since there does not seem to be uniform convergence - the spikes near T=60 are similar, but other regions have sign changes between refinements. Also, there could be precision errors, as OpenFoam has only been set to output 6 significant figures. Finally, the FDE (finite difference equation) used to calculate the strain rate may be inaccurate, since we used a first-order forward/backward difference for the left and right walls. This was done since only two OpenFoam samples were taken at each wall per timestep, but that may not have been sufficient.

Assuming that the above is accurate, the net force on the internal beams comprising those walls can be calculated as follows (in units of $\rho U^2 L^2$):

$$F = w * \tau = (0.1) * \tau = (0.1) * \mu * (stress\_rate)$$

Since these results are fairly questionable, we do not calculate an example.

7.13. Volumetric Flow Rate and Mixing

To investigate inflow/outflow rates, we will consider integration of a profile across the internal window opening (profile D on the mesh diagram).
Note that the meshFactor of 3 fails for Re=10000 again.

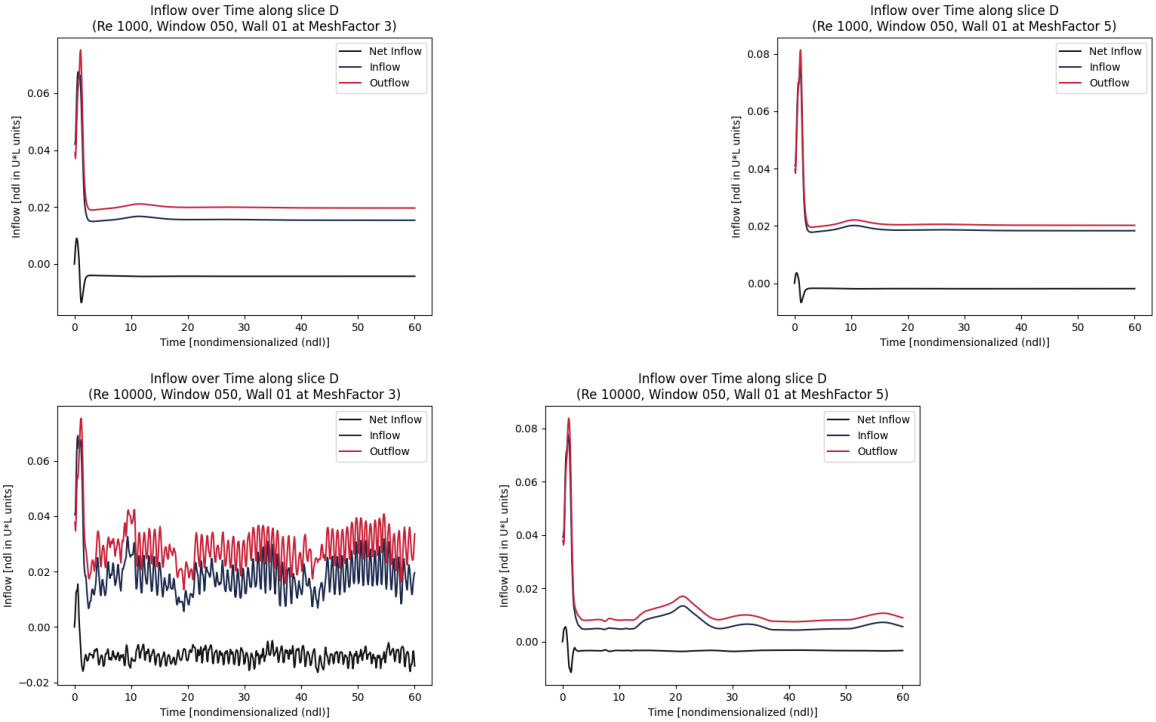

Looking at the net flow rate, clearly the cavity first pressurizes and then slowly depressurizes over time.
While this is happening, large amounts of fluid are still being cycled through the window - a huge amount in the first few timesteps (up to ~T=2), and then a somewhat large amount afterwards.

To visualize the scale, an example will be shown.

For a $1m^2$ window and $90km/hr (56mph)$ wind, approximately $(25m/s)(1)(1)(0.08) = 2m^3 persecond$ is cycled through in the first ~2 seconds!
Afterward, $0.25m^3/s$ is cycled in and out on average.
After the initial spike, there is a net decreasing outflow starting at $0.05m^3/s$ (using the Re=10000 plot).
Note this example is fairly realistic, since an EF0 tornado has slightly higher windspeed, and can be approximated as parallel streamline flow due to the large tornado radius.
While this example is not entirely accurate since the windspeed used can produce much higher Reynolds numbers in flow, the large-scale behavior is identical, as shown below.

Note that the maximum cycle flow rate of 8% freestream is consistent between both Reynolds numbers. From the previous analysis on Strouhal numbers, we see that since the large-scale flows are fairly Reynolds-number-independent, it is possible that the volumetric flowrate has converged, and will remain the same for higher Reynolds numbers.

If that is the case, then the low-Reynolds analysis can be combined with a couple of measurements of high-Reynolds flow, and extrapolated out to actual cases, providing an extremely useful tool for flow estimation.

A possible topic for further investigation would be the generation of fixed-Strouhal-number flow components with different Reynolds numbers. If the flow field can be seperated into higher frequency harmonics that are added with higher Reynolds number, then that would allow modeling of higher Reynolds flow primarily with low-Reynolds measurements.

8. Appendix

8.14. Mesh Images

Mesh Images for the Low Reynolds simulations (same order)

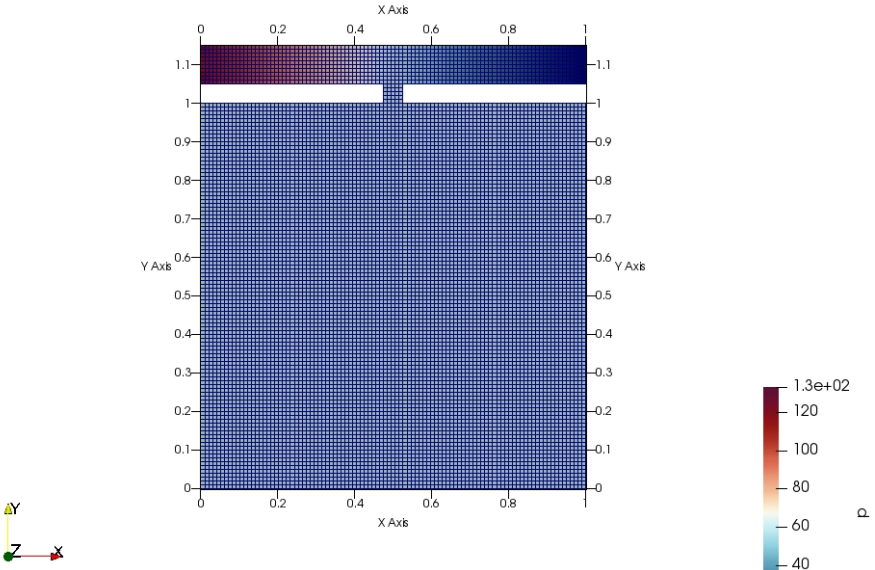
X Axis
Y Axis
p
1.3e+02
120
100
80
60
40
20
0.0e+00
Y
Z
X

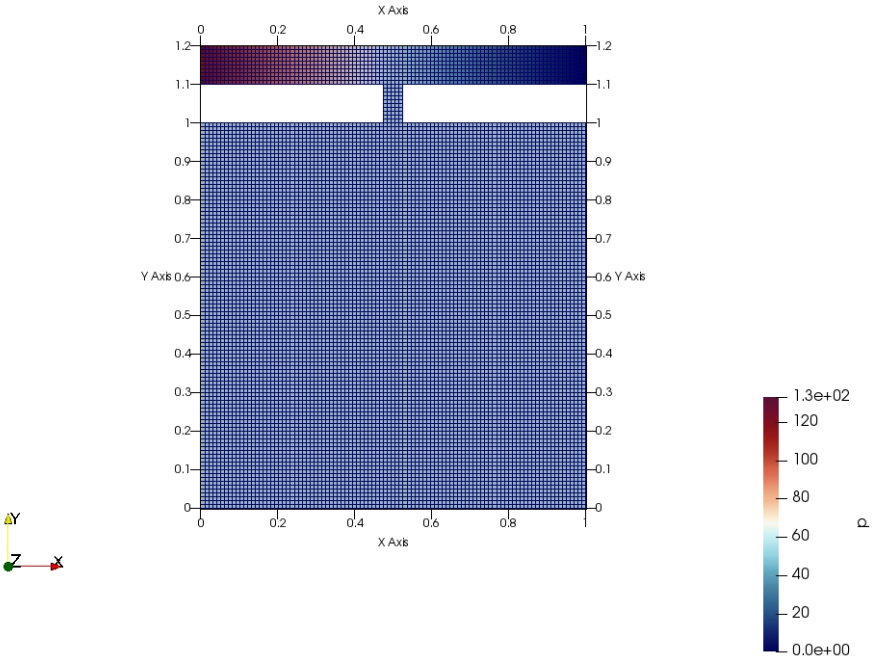
X Axis
Y Axis
p
1.3e+02
120
100
80
60
40
20
0.0e+00
Y
Z
X

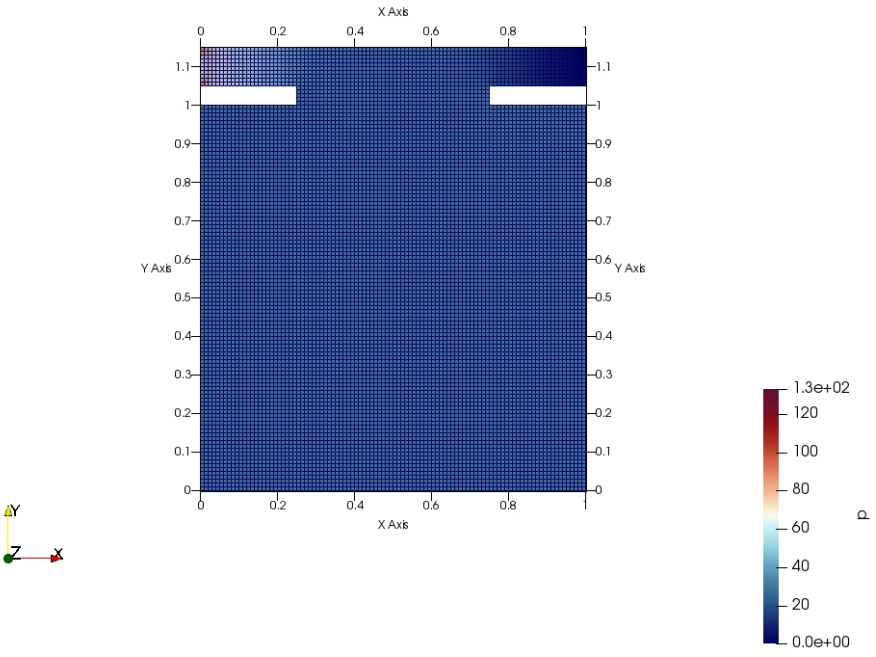
X Axis
Y Axis
0
0.2
0.4
0.6
0.8
1
1.1
0.9
0.7
0.5
0.3
0.1
Y
Z
X
1.3e+02
120
100
80
60
40
20
0.0e+00
p

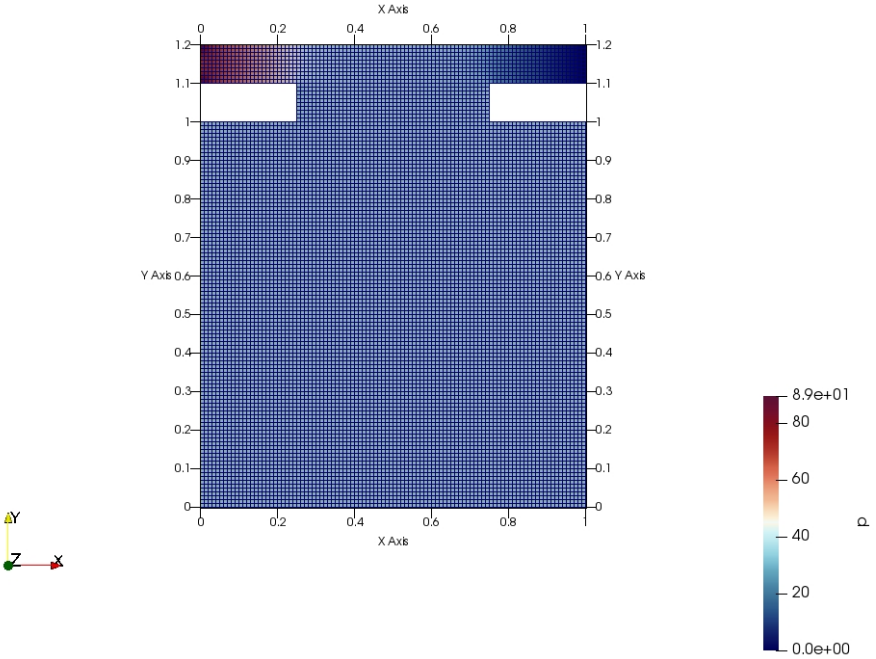
X Axis
Y Axis
0
0.2
0.4
0.6
0.8
1
1.2
1.1
0.9
0.7
0.5
0.3
0.1
Y
Z
X
8.9e+01
80
60
40
20
0.0e+00
p

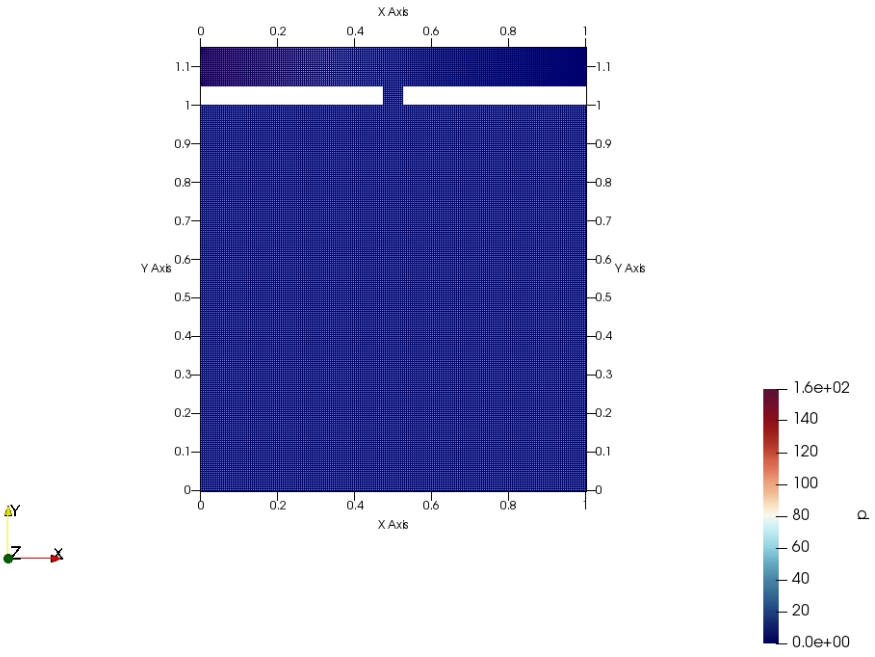
X Axis
Y Axis
0
0.2
0.4
0.6
0.8
1
1.1
0.9
0.7
0.5
0.3
0.1
Y
Z
X
1.6e+02
140
120
100
80
60
40
20
0.0e+00
p

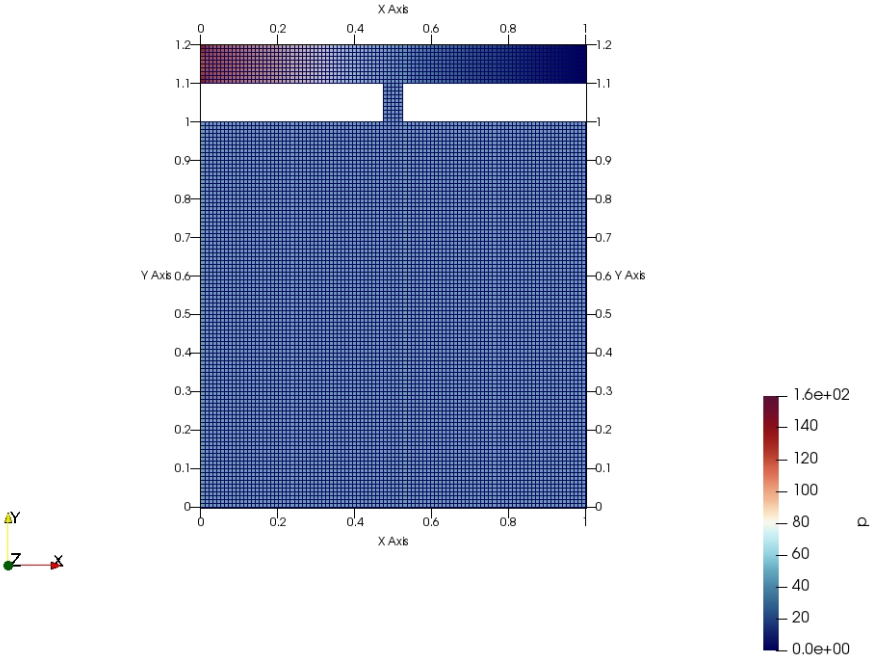
X Axis
Y Axis
0
0.2
0.4
0.6
0.8
1
1.2
1.1
0.9
0.7
0.5
0.3
0.1
Y
Z
X
1.6e+02
140
120
100
80
60
40
20
0.0e+00
p

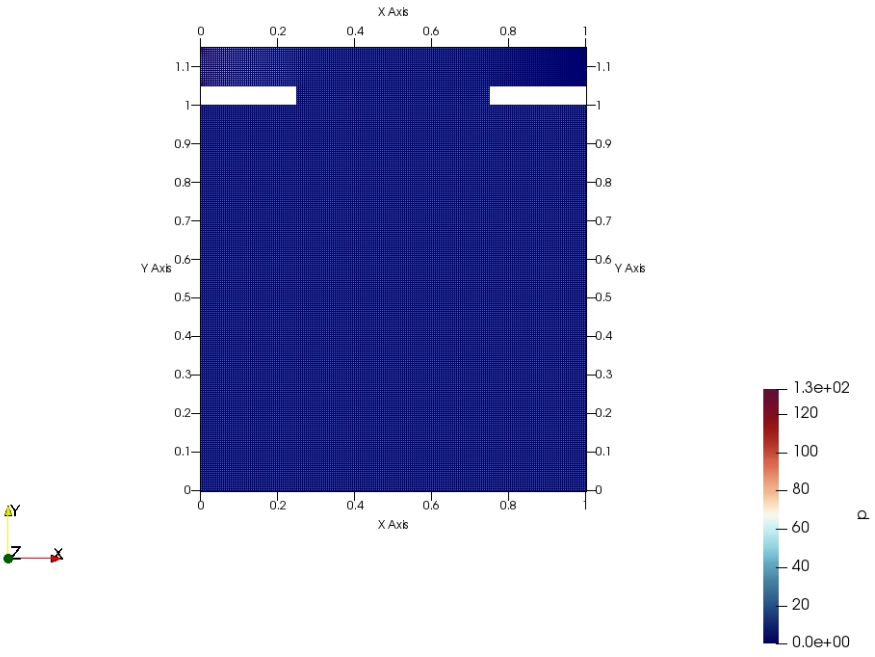
X Axis
Y Axis
0
0.2
0.4
0.6
0.8
1
1.1
0.9
0.7
0.5
0.3
0.1
Y
Z
X
1.3e+02
120
100
80
60
40
20
0.0e+00
p

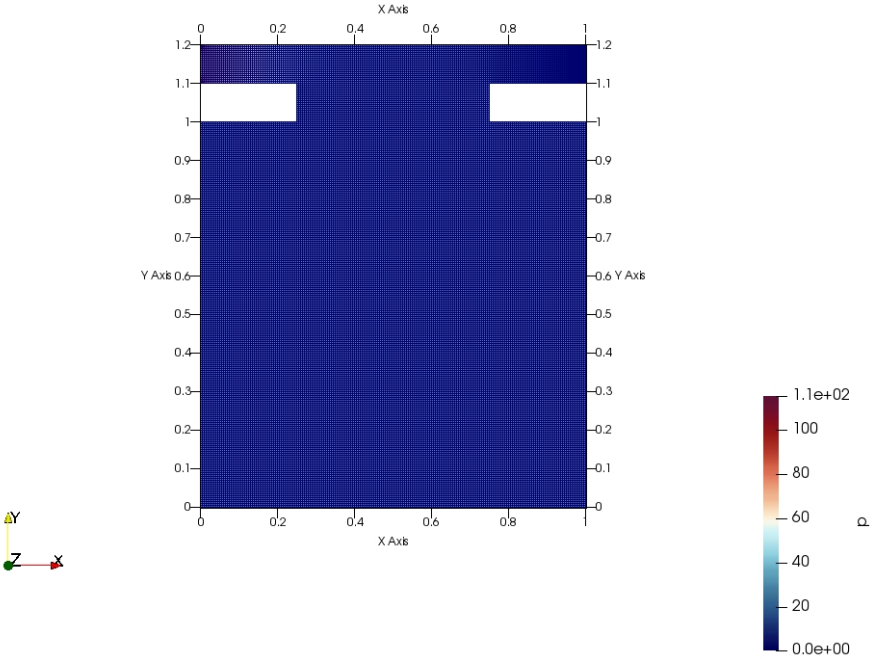
X Axis
Y Axis
0
0.2
0.4
0.6
0.8
1
1.2
1.1
0.9
0.7
0.5
0.3
0.1
Y
Z
X
1.1e+02
100
80
60
40
20
0.0e+00
p

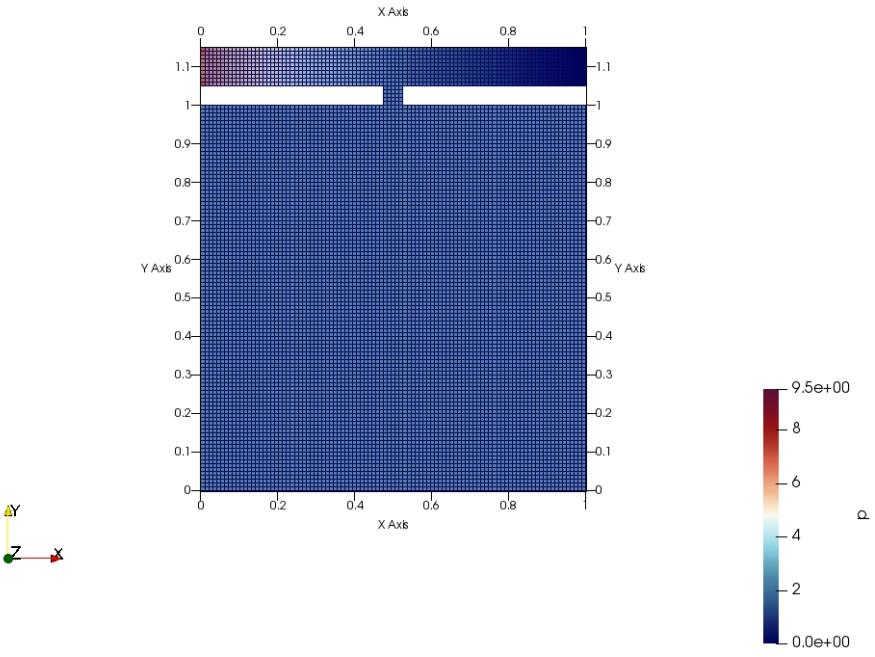
X Axis
Y Axis
0
0.2
0.4
0.6
0.8
1
1.1
0.9
0.7
0.5
0.3
0.1
Y
Z
X
9.5e+00
8
6
4
2
0.0e+00
p

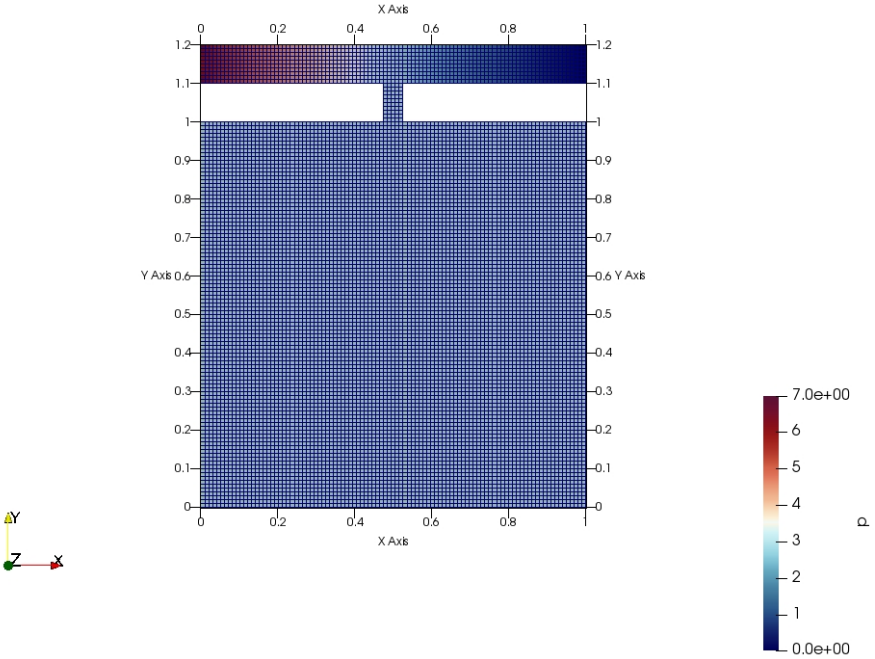
X Axis
Y Axis
0
0.2
0.4
0.6
0.8
1
1.2
1.1
0.9
0.7
0.5
0.3
0.1
Y
Z
X
7.0e+00
6
5
4
3
2
1
0.0e+00
p

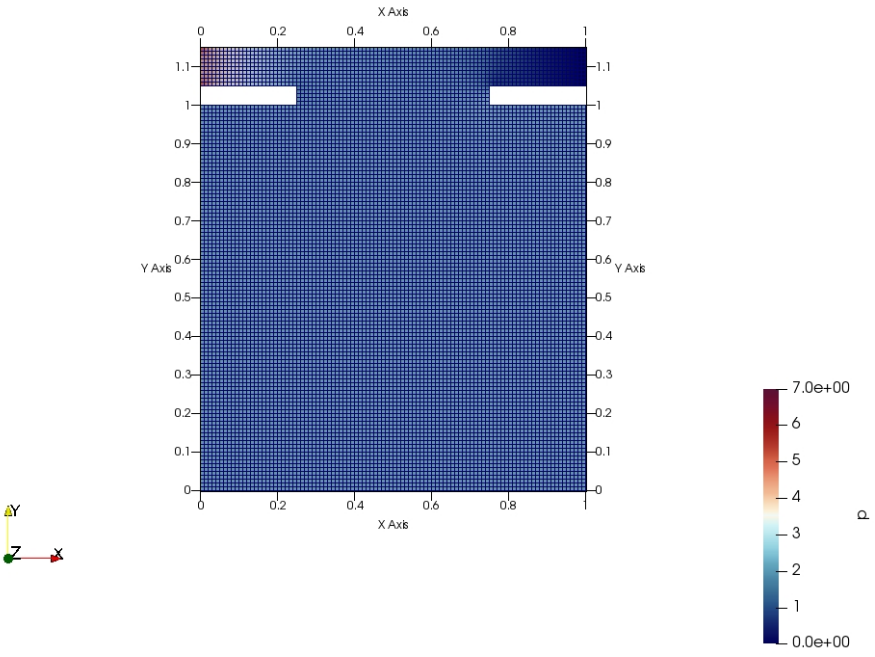
X Axis
Y Axis
Y Axis
X Axis
Y
Z
X
7.0e+00
6
5
4
3
2
1
0.0e+00
ρ

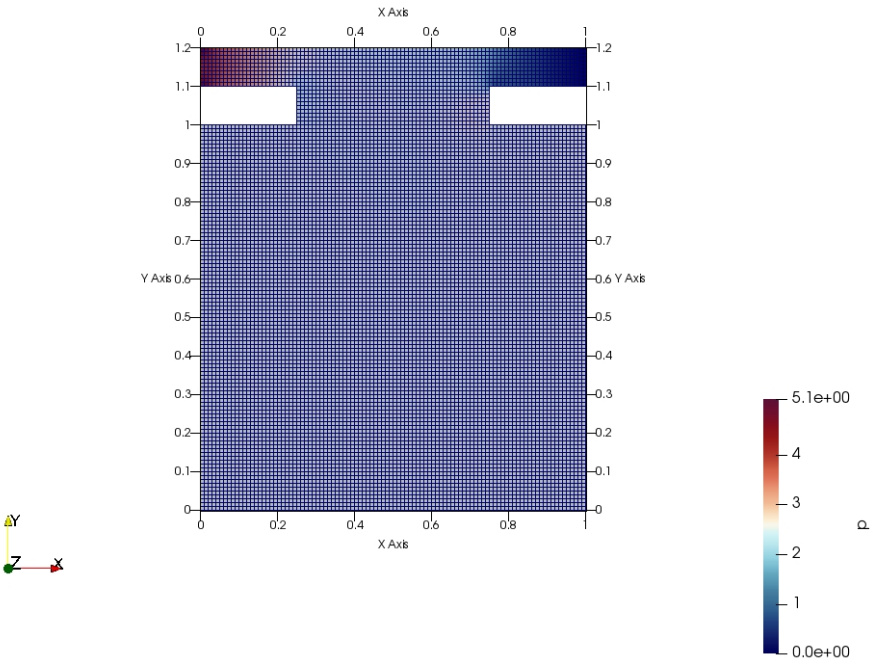
X Axis
Y Axis
Y Axis
X Axis
Y
Z
X
5.1e+00
4
3
2
1
0.0e+00
ρ

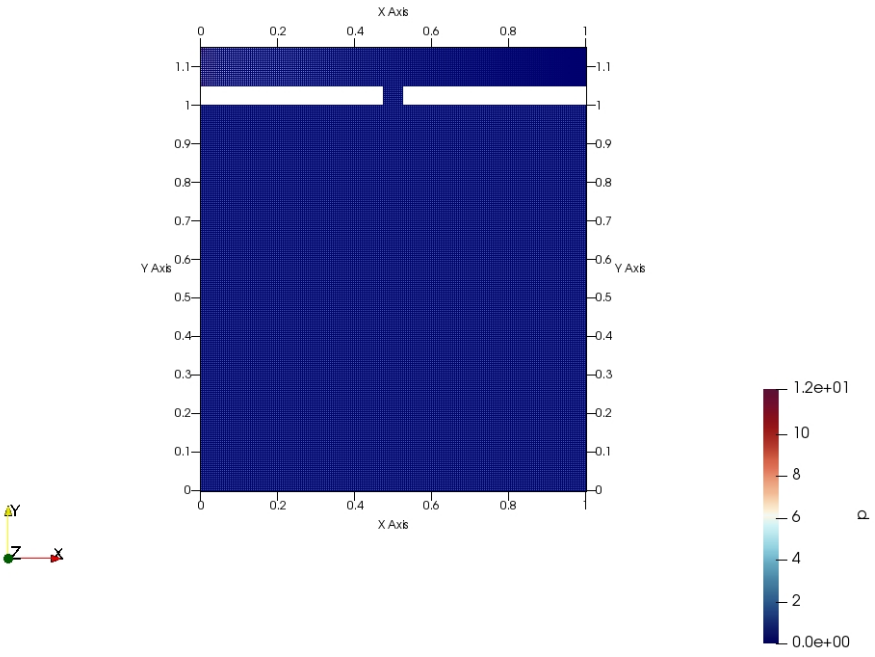
X Axis
Y Axis
0
0.2
0.4
0.6
0.8
1
1.1
0.9
0.7
0.5
0.3
0.1
Y
Z
X
1.2e+01
10
8
6
4
2
0.0e+00
p

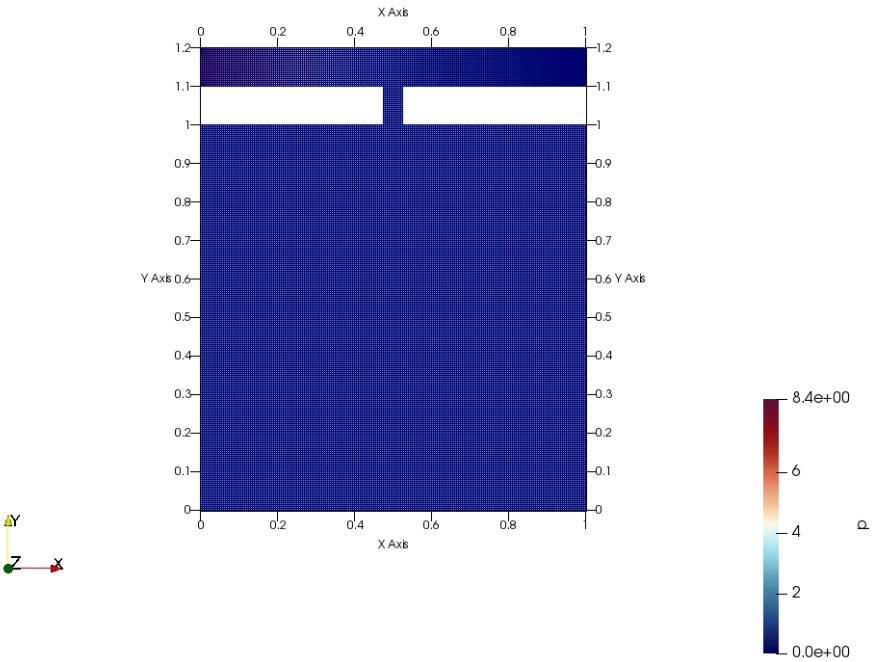
X Axis
Y Axis
0
0.2
0.4
0.6
0.8
1
1.2
1.1
0.9
0.7
0.5
0.3
0.1
Y
Z
X
8.4e+00
6
4
2
0.0e+00
p

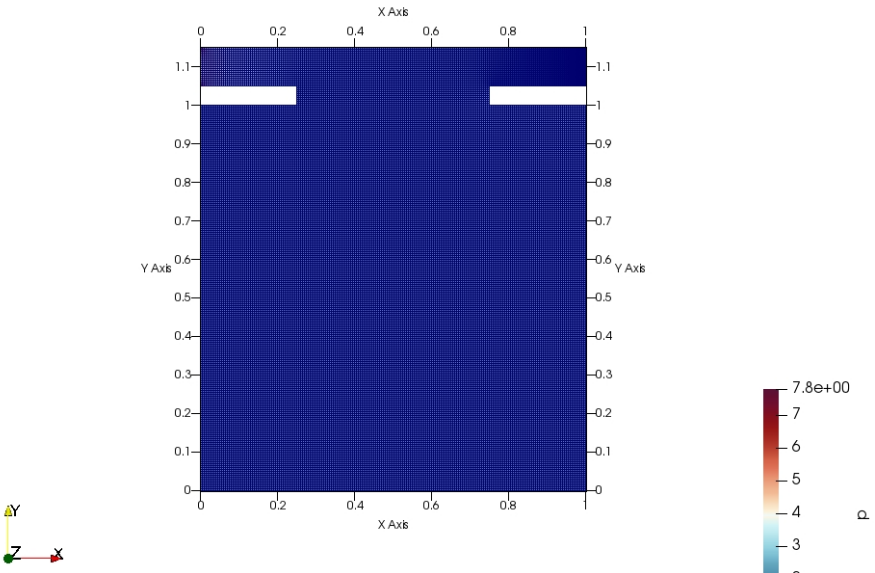

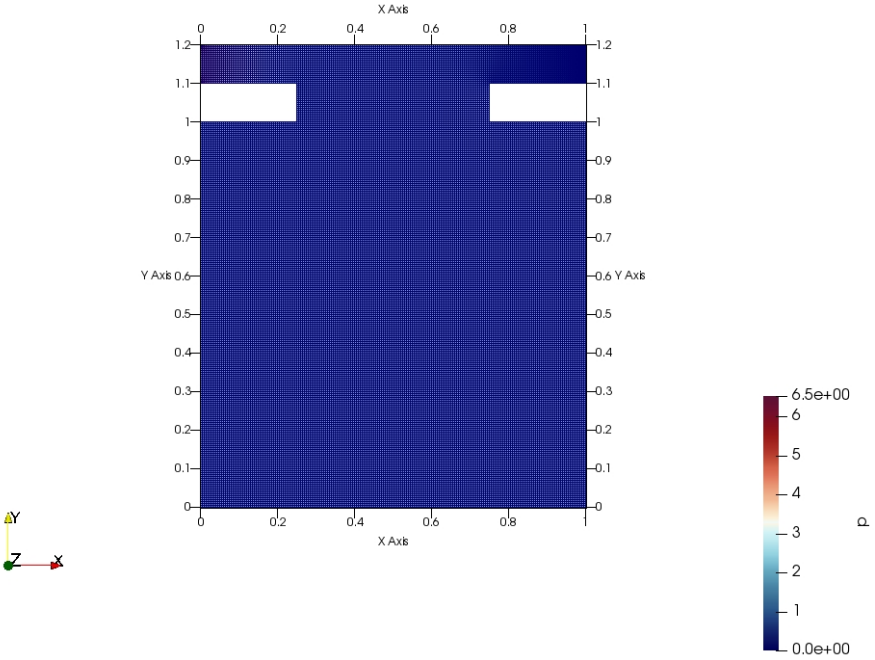

Mesh Images for the High Reynolds simulations (same order)

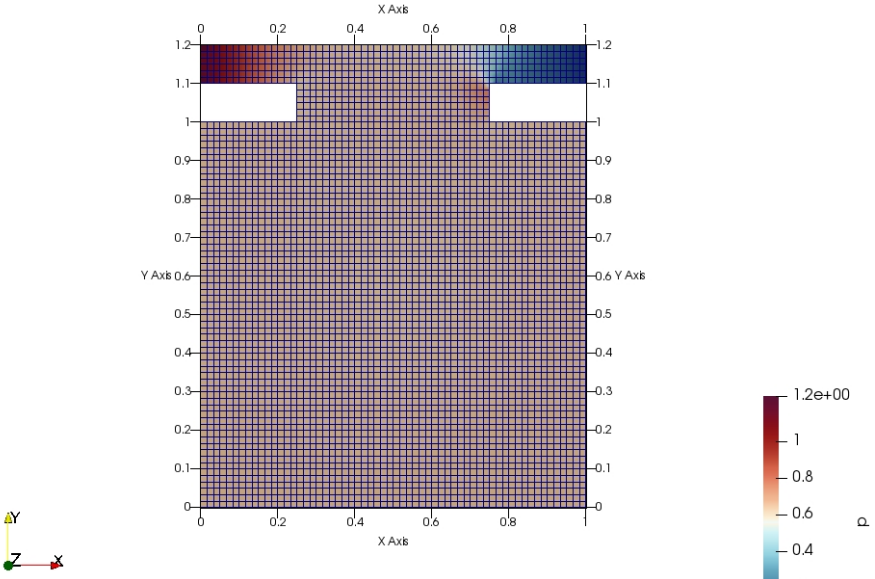
X Axis
Y Axis
0
0.2
0.4
0.6
0.8
1
1.2
1.1
0.9
0.7
0.5
0.3
0.1
Y
Z
X
1.2e+00
1
0.8
0.6
0.4
0.2
0
-1.5e-01
p

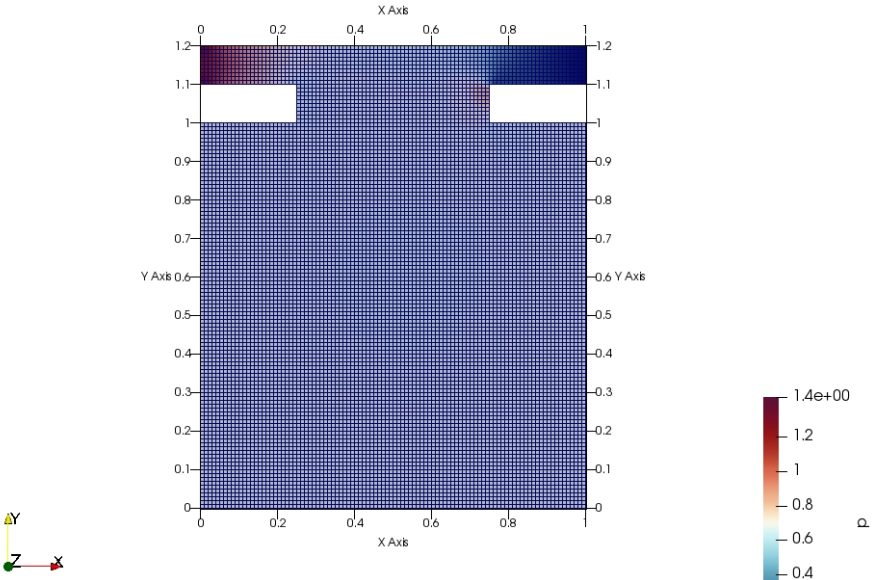
X Axis
Y Axis
0
0.2
0.4
0.6
0.8
1
1.2
1.1
0.9
0.7
0.5
0.3
0.1
Y
Z
X
1.4e+00
1.2
1
0.8
0.6
0.4
0.2
-5.0e-02
p

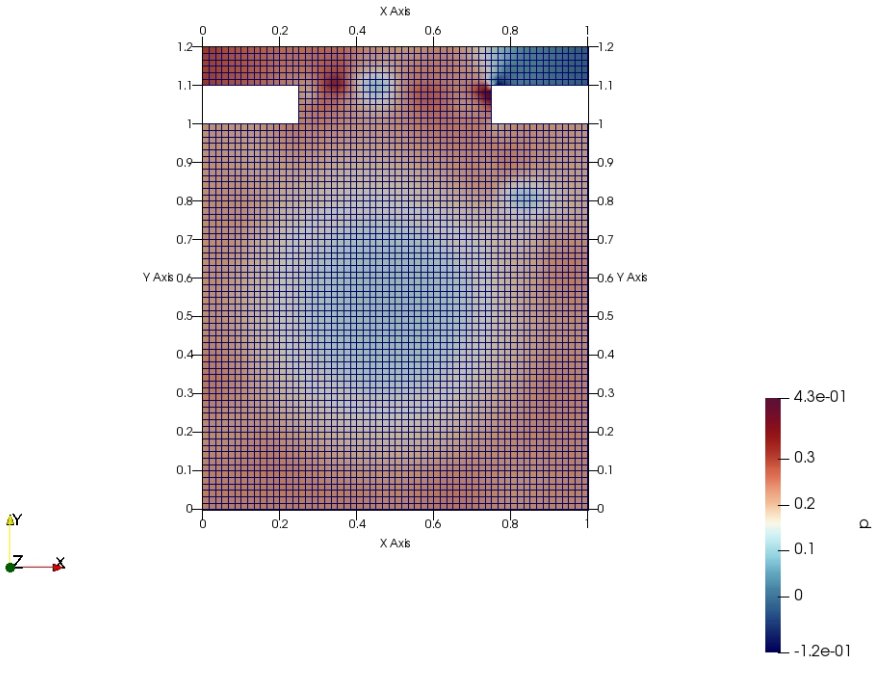

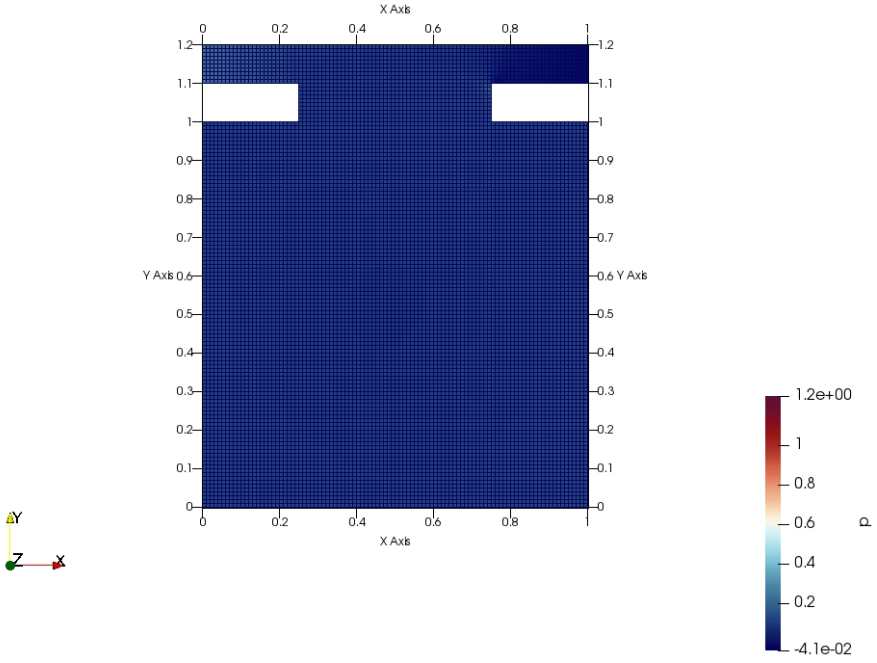

9. References

(2019, May). *Super Inspection Pros*. Retrieved from https://superinspectionpros.local:57400/blog/how-high-does-wind-speed-need-to-be-to-damage-a-home/

Allaire J, Xie Y, McPherson J, Luraschi J, Ushey K, Atkins A, Wickham H, Cheng J, Chang W, Iannone R (2021). *Rmarkdown: Dynamic Documents for r*. Retrieved from https://CRAN.R-project.org/package=rmarkdown

Bengtsson H (2021). *R.utils: Various Programming Utilities*. Retrieved from https://github.com/HenrikBengtsson/R.utils

Hadhazy A (2011, May). "How a Tornado Can Destroy a House." *Popular Mechanics*. Retrieved from https://www.popularmechanics.com/outdoors/survival/stories/gone-in-four-seconds-how-a-tornado-destroys-a-house

Kim HJ, Durbin PA (1988). "Observations of the Frequencies in a Sphere Wake and of Drag Increase by Acoustic Excitation." *The Physics of Fluids*, **31**(11), 3260–3265. https://doi.org/10.1063/1.866937.

Sakamoto H, Haniu H (1990). "A study on vortex shedding from spheres in a uniform flow." *ASME Journal of Fluids Engineering*, **112**, 386–392.

Tessner T (2021, August). "What Are Hurricane Shutters? An Introduction to Hurricane Shutters." *Eurex Shutters*. Retrieved from https://eurexshutters.com/what-are-hurricane-shutters/

Urbanek S (2021). *Jpeg: Read and Write JPEG Images*. Retrieved from http://www.rforge.net/jpeg/

Xie Y (2013). "animation: An R Package for Creating Animations and Demonstrating Statistical Methods." *Journal of Statistical Software*, **53**(1), 1–27. Retrieved from https://doi.org/10.18637/jss.v053.i01

Xie Y (2014). "Knitr: A Comprehensive Tool for Reproducible Research in R." In *Implementing reproducible computational research*, eds. V Stodden, F Leisch, and RD Peng,. Chapman; Hall/CRC. Retrieved from http://www.crcpress.com/product/isbn/9781466561595

Xie Y (2015). *Dynamic Documents with R and Knitr* 2nd ed. Chapman; Hall/CRC, Boca Raton, Florida. Retrieved from https://yihui.org/knitr/

Xie Y (2021a). *Animation: A Gallery of Animations in Statistics and Utilities to Create Animations*. Retrieved from https://yihui.org/animation/

Xie Y (2021b). *Knitr: A General-Purpose Package for Dynamic Report Generation in r*. Retrieved from https://yihui.org/knitr/

Xie Y, Allaire JJ, Grolemund G (2018). *R Markdown: The Definitive Guide*. Chapman; Hall/CRC, Boca Raton, Florida. Retrieved from https://bookdown.org/yihui/rmarkdown

Xie Y, Dervieux C, Riederer E (2020). *R Markdown Cookbook*. Chapman; Hall/CRC, Boca Raton, Florida. Retrieved from https://bookdown.org/yihui/rmarkdown-cookbook

10. Acknowledgements

Thank you so much for reading this work!

Affiliation:

Justin Campbell
Aerospace Department, University of Texas at Austin
E-mail: Campbelljustin989@gmail.com - jsc4348

Affiliation:

Amanda Hiett
Aerospace Department, University of Texas at Austin
E-mail: hiett.mandy@utexas.edu - amh7427

Affiliation:

Akhil Sadam
Aerospace Department, University of Texas at Austin
E-mail: akhil.sadam@utexas.edu - as97822

Journal of Statistical Software http://www.jstatsoft.org/
published by the Foundation for Open Access Statistics http://www.foastat.org/
MMMMMM YYYY, Volume VV, Issue II *Submitted:* yyyy-mm-dd
doi: 10.18637/jss.v000.i00 *Accepted:* yyyy-mm-dd